Journal Pre-proof

Dihydromyricetin mitigates abdominal aortic aneurysm *via* transcriptional and post-transcriptional regulation of heme oxygenase-1 in vascular smooth muscle cells

Weile Ye, Pinglian Yang, Mei Jin, Jiami Zou, Zhihua Zheng, Yuanyuan Li, Dongmei Zhang, Wencai Ye, Zunnan Huang, Jiaojiao Wang, Zhiping Liu

PII: S2211-3835(25)00036-X

DOI: https://doi.org/10.1016/j.apsb.2025.02.003

Reference: APSB 2253

To appear in: *Acta Pharmaceutica Sinica B*

Received Date: 10 July 2024

Revised Date: 15 September 2024

Accepted Date: 26 November 2024

Please cite this article as: Ye W, Yang P, Jin M, Zou J, Zheng Z, Li Y, Zhang D, Ye W, Huang Z, Wang J, Liu Z, Dihydromyricetin mitigates abdominal aortic aneurysm *via* transcriptional and post-transcriptional regulation of heme oxygenase-1 in vascular smooth muscle cells, *Acta Pharmaceutica Sinica B*, https://doi.org/10.1016/j.apsb.2025.02.003.

Original article

Dihydromyricetin mitigates abdominal aortic aneurysm *via* transcriptional and post-transcriptional regulation of heme oxygenase-1 in vascular smooth muscle cells

Weile Ye[a,†], Pinglian Yang[a,†], Mei Jin[a,†], Jiami Zou[a], Zhihua Zheng[a], Yuanyuan Li[a], Dongmei Zhang[a], Wencai Ye[a], Zunnan Huang[b,*], Jiaojiao Wang[b,*], Zhiping Liu[a,*]

[a]*State Key Laboratory of Bioactive Molecules and Druggability Assessment, Guangdong Province Key Laboratory of Pharmacodynamic Constituents of TCM and New Drugs Research, International Cooperative Laboratory of Traditional Chinese Medicine Modernization and Innovative Drug Discovery of Chinese Ministry of Education (MOE), College of Pharmacy, Jinan University, Guangzhou 511436, China*

[b]*Key Laboratory of Big Data Mining and Precision Drug Design of Guangdong Medical University, Key Laboratory of Computer-Aided Drug Design of Dongguan City, Key Laboratory for Research and Development of Natural Drugs of Guangdong Province, School of Pharmacy, Guangdong Medical University, Dongguan 523808, China*

Received 10 July 2024; received in revised form 15 September 2024; accepted 26 November 2024

*Corresponding authors.

E-mail addresses: zhiping0414@163.com (Zhiping Liu), zn_huang@gdmu.edu.cn (Zunnan Huang), jjwang89@163.com (Jiaojiao Wang).

[†]These authors made equal contributions to this work.

Running title: Dihydromyricetin mitigates abdominal aortic aneurysm *via* HO-1

Graphical abstract

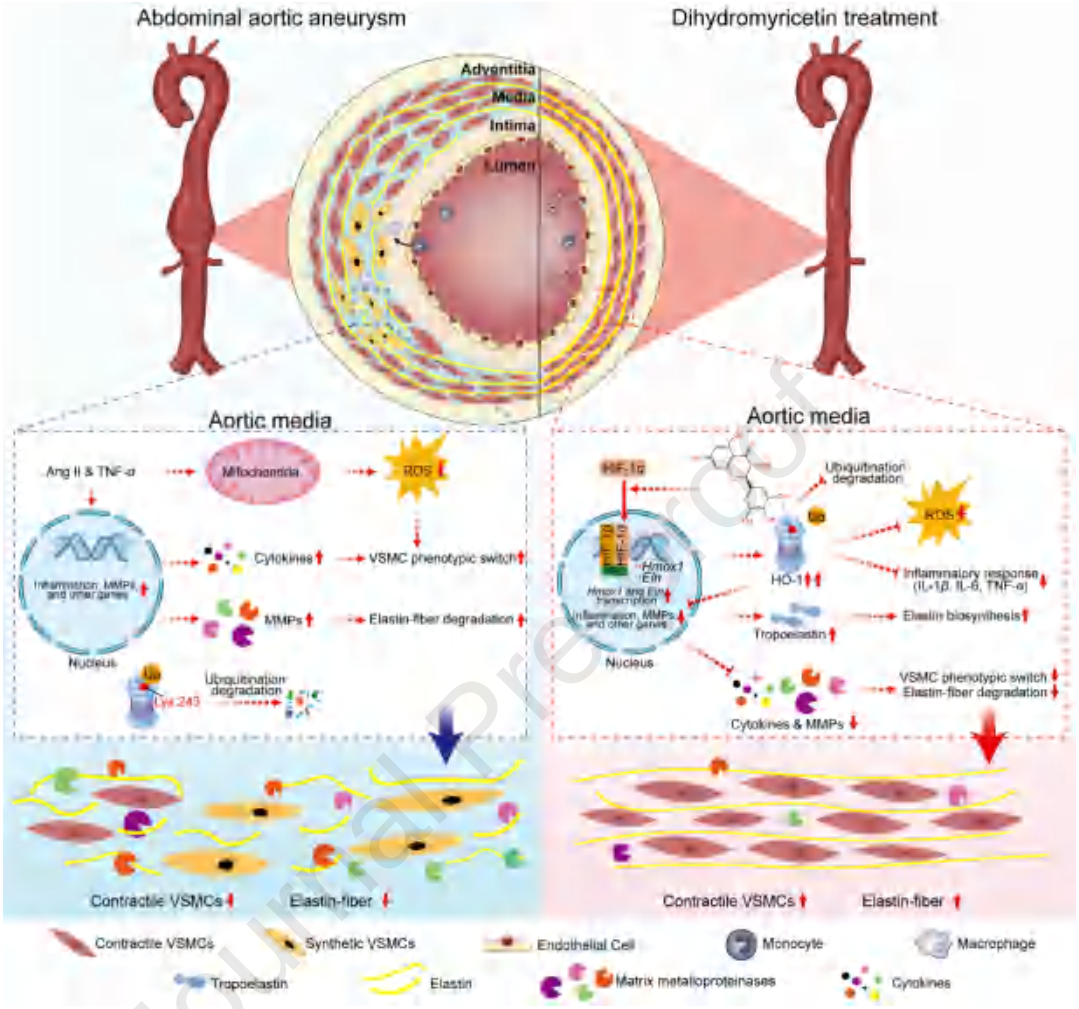

Dihydromyricetin alleviates AAA by suppressing VSMC inflammation and ROS production, while preserving VSMC contractile phenotype through inducing HIF-1α-mediated HO-1 transcription and inhibiting HO-1 ubiquitination by binding to HO-1 at Lys243.

Original article

Dihydromyricetin mitigates abdominal aortic aneurysm *via* transcriptional and post-transcriptional regulation of heme oxygenase-1 in vascular smooth muscle cells

Weile Ye[a,†], Pinglian Yang[a,†], Mei Jin[a,†], Jiami Zou[a], Zhihua Zheng[a], Yuanyuan Li[a], Dongmei Zhang[a], Wencai Ye[a], Zunnan Huang[b,*], Jiaojiao Wang[b,*], Zhiping Liu[a,*]

[a]*State Key Laboratory of Bioactive Molecules and Druggability Assessment, Guangdong Province Key Laboratory of Pharmacodynamic Constituents of TCM and New Drugs Research, International Cooperative Laboratory of Traditional Chinese Medicine Modernization and Innovative Drug Discovery of Chinese Ministry of Education (MOE), College of Pharmacy, Jinan University, Guangzhou 511436, China*

[b]*Key Laboratory of Big Data Mining and Precision Drug Design of Guangdong Medical University, Key Laboratory of Computer-Aided Drug Design of Dongguan City, Key Laboratory for Research and Development of Natural Drugs of Guangdong Province, School of Pharmacy, Guangdong Medical University, Dongguan 523808, China*

Received 10 July 2024; received in revised form 15 September 2024; accepted 26 November 2024

*Corresponding authors.

E-mail addresses: zhiping0414@163.com (Zhiping Liu), zn_huang@gdmu.edu.cn (Zunnan Huang), jjwang89@163.com (Jiaojiao Wang).

[†]These authors made equal contributions to this work.

Running title: Dihydromyricetin mitigates abdominal aortic aneurysm *via* HO-1

Abstract Abdominal aortic aneurysm (AAA) is a deadly condition of the aorta, carrying a significant risk of death upon rupture. Currently, there is a dearth of efficacious pharmaceutical interventions to impede the advancement of AAA and avert it from rupturing. Here, we investigated dihydromyricetin (DHM), one of the predominant bioactive flavonoids in *Ampelopsis grossedentata* (*A. grossedentata*), as a potential agent for inhibiting AAA. DHM effectively blocked the formation of AAA in angiotensin II-infused apolipoprotein E-deficient ($ApoE^{-/-}$) mice. A combination of network pharmacology and whole transcriptome sequencing analysis revealed that DHM's anti-AAA action is linked to heme oxygenase (HO)-1 (*Hmox-1* for the rodent gene) and hypoxia-inducible factor (HIF)-1α in vascular smooth muscle cells (VSMCs).

Remarkably, DHM caused a robust rise (~10 fold) of HO-1 protein expression in VSMCs, thereby suppressing VSMC inflammation and oxidative stress and preserving the VSMCs contractile phenotype. Intriguingly, the therapeutic effect of DHM on AAA was largely abrogated by VSMC-specific *Hmox1* knockdown in mice. Mechanistically, on one hand, DHM increased the transcription of *Hmox-1* by triggering the nuclear translocation and activation of HIF-1α, but not nuclear factor erythroid 2-related factor 2 (NRF2). On the other hand, molecular docking, combined with cellular thermal shift assay (CETSA), isothermal titration calorimetry (ITC), drug affinity responsive target stability (DARTS), co-Immunoprecipitation (Co-IP), and site mutant experiments revealed that DHM bonded to HO-1 at Lys243 and prevented its degradation, thereby resulting in considerable HO-1 buildup. In summary, our findings suggest that naturally derived DHM has the capacity to markedly enhance HO-1 expression in VSMCs, which may hold promise as a therapeutic strategy for AAA.

KEY WORDS Flavonoids; Dihydromyricetin; Abdominal aortic aneurysm; Vascular smooth muscle cells; Heme oxygenase-1; HIF-1α; Inflammation; Oxidative stress

1. Introduction

Abdominal aortic aneurysm (AAA), the predominant form of aneurysm, is distinguished by enduring and irreversible regional expansion of the abdominal aorta, typically exhibiting an asymptomatic condition[1,2]. Nonetheless, aneurysm rupture is frequently fatal, with a mortality rate exceeding 90%[3]. Pathologically characterized by aortic wall inflammation, smooth muscle cell (SMC) phenotypic switching, and extracellular matrix (ECM) degradation[4-6], AAA was attributable to 167,200 fatalities and 3 million disability-adjusted life years globally in 2017[7]. While surgical interventions can reduce the risk of life-threatening rupture in large AAAs in the short term, they have shown no significant impact on long-term patient survival[8]. The alarming fact is that there's currently a lack of effective pharmaceutical interventions to halt the progression and eventual rupture of AAA[3]. Consequently, there's a pressing need to advance new pharmaceuticals targeting AAA to make significant strides in the field of medical therapeutics.

A. grossedentata is an herb possessing medical and edible peculiarities, and its stems and leaves have been practiced for centuries as a medicinal tea known as vine tea, which is traditionally used to prevent and treat the common cold, sore throat, stab wounds, and icteric viral hepatitis[9]. At present, 20 distinct flavonoids from vine tea have

been successfully isolated and identified[9]. Among them, dihydromyricetin (DHM) is one of the predominant bioactive flavonoids and accounts for the highest proportion (20%–30%, *w*/*w*) of flavonoids in *A. grossedentata*[10,11], exhibiting a diverse range of biological and pharmacological properties (*e.g.*, antioxidant, anti-inflammatory, lipid and blood glucose regulatory)[12-15] and cardiovascular protective effects[16-18], indicating that it may have potential as an anti-AAA compound. However, direct evidence regarding the inhibitory effects of DHM on AAA is still lacking.

Heme oxygenase (HO)-1 is a stress-responsive protein situated downstream of the transcription factors nuclear factor erythroid 2-related factor 2 (NRF2) and hypoxia inducible factor (HIF)-1α[19], whose primary function is to enhance the enzymatic degradation of heme into bioactive compounds that possess potent anti-inflammatory and antioxidant properties, thereby inhibiting the synthesis of matrix metalloproteinases (MMPs)[20-23]. Elevating HO-1 levels has a prophylactic impact on non-ruptured human AAA[24], aligning with studies indicating that a deficiency in HO-1 exacerbates Ang II-induced aortic aneurysm in mice[25]. Although the NRF2/HO-1 signaling pathway is recognized as one of the regulatory mechanisms for drug therapy targeting AAA[26-28], an increasing number of studies have shed light on the significance of the HIF-1α signaling pathway in AAA *via* promoting elastin fiber formation and tissue inhibitors of metalloproteinase expression[29,30]. HIF-1α orchestrates intricate signaling networks by interacting with various upstream and downstream proteins, playing a pivotal role in the regulation of both physiological and pathological processes, as well as in the growth, development, and homeostasis of the organism[31]. Consequently, targeting the HIF-1α/HO-1 signaling axis to boost elastin fiber formation and HO-1 expression appears to hold promise for treating AAA.

In this study, we utilized the Ang II-induced murine AAA model, combined network pharmacology, RNA sequencing, chromatin immunoprecipitation assay (ChIP), cellular thermal shift assay (CETSA), drug affinity responsive target stability (DARTS), co-Immunoprecipitation (Co-IP), isothermal titration calorimetry (ITC), *in vivo* SMC-specific *Hmox1* gene knockdown, and an *in vitro* pharmacological inhibitor to comprehensively explore the role of DHM on AAA and the underlying mechanisms. Our findings, for the first time, indicated that DHM prevented the formation of AAA in Ang II-induced ApoE$^{-/-}$ mice *via* robust induction of HO-1 expression. Mechanistically, we found that DHM was directly binding to Lys243 of the HO-1 protein connected to inhibit ubiquitination. In addition, DHM promoted transcription

factor HIF-1α nuclear translocation and activation, thus leading to transcriptional induction of HO-1 and other target genes in VSMCs.

2. Materials and methods

2.1. Reagents and antibodies

DHM powder ($C_{15}H_{12}O_8$, > 98% pure, S24435), myricetin powder (MYR, $C_{15}H_{10}O_8$, B21458), and polydatin powder (PD, $C_{20}H_{22}O_8$, B20533) were purchased from Shanghai Yuanye Biotechnology Company (China). Shanghai Macklin Biochemical Technology Company Limited (China) provided doxycycline hyclate powder (DOXY, $C_{22}H_{24}N_2O_8HCl$, D824282), naringenin powder (NAR, $C_{15}H_{12}O_5$, N875513), and imidazole ($C_3H_4N_2$, I823673). Ginsenoside Rg1 (RG1, $C_{42}H_{72}O_{14}$, A0237) was obtained from Chengdu Must Bio-Technology Company Limited (China). Zinc Protoporphyrin (ZnPPIX, $C_{34}H_{32}N_4O_4Zn$, MB4231) was purchased from MeilunBio® (China). Angiotensin II (Ang II, ALX-151-039) was obtained from Enzo Life Sciences (USA). ALZET® osmotic pumps (model 2004) were from Durect Corporation (USA). TNF-α (300-01A) was from PeproTech (USA). Cell Counting Kit-8 (CCK-8-100) was from GBCBIO Biotechnology Company (China). Isopropyl β-D-thiogalactoside (HM-IG25) was from Haoma Biotechnology Company Limited (China). Antibodies are listed in Supporting Information Table S1. Dylight 649, Goat Anti-Rabbit IgG (A23620) and Dylight 488, Goat Anti-Mouse IgG (A23210) were purchased from Abbkine Scientific Company Limited (China). TNF-α, IL-1β, and IL-6 ELISA kits (EMC102a, EMC001b and EMC004) were obtained from NeoBioscience Technology Company Limited (China).

2.2. Animals experiment

Male ApoE$^{-/-}$ mice (30 ± 2 g) aged 12-week-old were purchased from the Gempharmatech Company (China). All mice received full access to food and water while being subjected to a 12-h light/dark cycle under predetermined ambient conditions at 25 ± 2 °C with a relative humidity of 50%. The animal experiments were approved by the Institutional Animal Care and Use Committee (Approval No. IACUC-20230625-12), and they were carried out in line with the Chinese Animal Welfare Law.

After being adaptively fed for one week, mice were randomly divided into four groups as follows: (1) Saline group (Saline); (2) Model group (Model); (3) Low-dose DHM treatment group (DHM-L); and (4) High-dose DHM treatment group (DHM-H),

n = 15 per group. The murine AAA model was replicated following established procedures as reported previously[32,33]. In brief, osmotic mini-pumps loaded with Ang II or saline were subcutaneously implanted in ApoE$^{-/-}$ mice, delivering Ang II at a rate of 1000 ng/kg/min over a 28-day period. On the day of the AAA model set up, DHM was administered to the mice *via* oral gavage at either a low dose (125 mg/kg) or a high dose (250 mg/kg) once daily, continuing for 28 days. The dose gradient of DHM was determined based on previous research[17,34,35]. Studies[17,34-36] have shown that the high dose of 250 mg/kg DHM protects the liver, improves atherosclerosis and attenuates diabetic cardiomyopathy without showing side effects. In contrast, mice in both the Saline group and the Model group received 0.5% carboxymethylcellulose sodium (CMC-Na, MB1731, MeilunBio®, China) through oral gavage. Testing mouse systolic blood pressure (SBP) in Weeks 0 and 4 following the Ang II infusion using a noninvasive tail-cuff blood pressure measuring device (BP-2000, Visitech Systems, Inc., USA). After the 28-day treatment period, the mice were euthanized using an overdose of sodium pentobarbital, and their aortas were subsequently harvested for analysis. A digital caliper was used to evaluate the abdominal aorta's maximum diameter in a double-blind fashion following Ang II infusion. An aortic dilatation of more than 50% of the normal aorta was classified as an aneurysm[37]. The ruptured aorta was taken into account when analyzing aneurysm incidence but not when analyzing aortic diameter.

Small short hairpin RNA (shRNA) specific to *Hmox1* was cloned and bundled into an adeno-associated viral (AAV) serotype 2 vector carrying the SMC-specific SM22α promoter to achieve SMC-specific knockdown of *Hmox1* in mice. All viruses were purchased from Vigene Biosciences Company Limited (China). AAV vectors containing the sh*Hmox1* coding sequence (AGCCACACAGCACTATGTAAA) along with green fluorescent protein (GFP), as well as control viruses carrying only GFP, through tail vein injections into ApoE$^{-/-}$ mice. Each mouse received a dose of 5×10^{11} vector genomes. Two weeks following the tail vein injection, the murine AAA model was established as mentioned above, and the mice were subsequently treated with 0.5% CMC-Na or a high dose of DHM.

2.3. Histological analysis

Abdominal aortas were promptly frozen in OCT compound or fixed and embedded in paraffin after being separated and washed with cold phosphate buffer solution (PBS).

Hematoxylin and eosin (H&E) were used to stain overall morphology; Verhoeff-Van Gieson (VVG) was used to stain elastin breakdown; and Masson's trichrome was used to stain collagen content in paraffin-embedded sections (4 μm thick). The number of breaks per vessel was used to calculate the amount of elastin degradation. Double-blind grading of the aortic elastin degradation was conducted using the following criteria: 1, less than 25% degradation; 2, between 25% and 50%; 3, between 50% and 75%; and 4, greater than 75% degradation.

2.4. Cell isolation, culture and treatments

The isolation and cultivation of rat bone marrow-derived macrophages (RBMDMs) were performed according to protocols described previously[38,39]. RBMDMs were cultured at 37 °C with 5% CO_2 in RPMI 1640 medium (CR-31800, Cienry, China) supplemented with 10% fetal bovine serum (FBS, AB-FBS-1050S, Xiamen Mogengel Biotechnology Company Limited, China), 20% L929 medium, and 1% penicillin–streptomycin (C0222, Beyotime Institute of Biotechnology, China). Rat aortic endothelial cells (RAECs) were extracted and pooled according to the procedure described previously[40,41] and cultured in Endothelial Cell Medium (ECM-1001, ScienCell, USA). Experiments were carried out on RAECs at passages 1 to 3. Rat aortic smooth muscle cells (RASMCs) were isolated from the abdominal aorta of male Sprague–Dawley rats and cultured as described[42]. In brief, the rat abdominal aorta was isolated and rinsed in cold PBS. After the endothelium and adventitia were removed, the aorta was cut into 1–2 mm pieces and plated in cell culture dishes. RASMCs were cultured in Dulbecco's modified Eagle's medium (DMEM, CR-12800, Cienry, China) supplemented with 10% FBS and 1% penicillin/streptomycin for at least 15 days until they reached confluence. Mouse aortic smooth muscle cells (MASMCs) were isolated and cultured according to the protocol previously described by us[33,43]. Briefly, after CO_2-induced euthanasia, sterile PBS perfusion excised the aortas. Trim excess connective tissue, immerse aortas in HBSS (#24020, Gibco, Ireland) with collagenase II (LS004176, Worthington Biochemical, USA), elastase (#2279, Worthington Biochemical, USA), and soybean trypsin inhibitor (#3571, Worthington Biochemical, USA), and incubate at 37 °C in 5% CO_2 for 8 min. After removing adventitia and stripping endothelial cells with forceps, the medial layers were digested with an enzyme solution for 1 h under the same circumstances. The resulting MASMCs were grown in DMEM with 20% FBS. After the identification of RASMCs and MASMCs by

morphology and immunofluorescence, the 3–6-generation cells were selected for experiments. In some experiments, cells were incubated with different concentration of DHM and other traditional Chinese medicine monomers, 10 ng/mL TNF-*α*, 50 μmol/L cycloheximide (CHx, HY-12320, MedChem Express, USA), 20 μmol/L MG132 (C2211, Sigma–Aldrich, USA), 10 μmol/L ML385 (846557-71-9, Target Molecule Corporation, China), 20 μmol/L LW 6 (HY-13671, MedChem Express, USA) or 10 μmol/L ZnPPIX at the indicated time points.

2.5. Network pharmacology

A total of 3214 *Homo sapiens* targets associated with DHM were searched from the OMIM (https://omim.org/), Digenet (https://www.disgenet.org/), and Genecards (https://www.genecards.org/) databases, with individual counts of 509, 543, and 2162 from each respective database. After eliminating duplicates, 2522 unique targets remained in connection with AAA. For DHM-related targets, 7, 75, and 387 targets were looked through the TCMSP (http://tcmspnw.com/), SwissTargetPrediction (http://swisstargetprediction.ch/), and Pharmmapper (http://www.lilab-ecust.cn/pharmmapper/) databases in that order. After getting rid of the copies, 424 DHM-related targets were found. Utilizing Cytoscape 3.10.0 software and its stringApp, we constructed two target networks pertaining to AAA and DHM. The intersection of these networks was analyzed, identifying key nodes with degree values exceeding 1.5 times the average. Through the OmicShare Platform, these intersection nodes of AAA and DHM underwent enrichment analysis, including Disease Ontology (DO), Kyoto Encyclopedia of Genes and Genomes (KEGG), and Gene Ontology (GO), and were visually represented with bar charts or bubble charts.

2.6. RNA-sequencing (RNA-seq)

Total RNA isolation was conducted on RASMCs exposed to TNF-*α* and treated with either dimethyl sulfoxide (DMSO) or DHM using Trizol reagent (15596018, Invitrogen, USA). The DMSO treatment group served as the control. Subsequently, 1–2 μg of total RNA was subjected to whole transcriptome RNA-seq analysis, which was performed through the Omicsmart high-throughput sequencing service in China. The *P*-value calculation was carried out using the false discovery rate method as implemented in the R package DESeq2. Differences in mRNA expression levels were depicted in a volcano plot, and further analyses, including GO and KEGG, were conducted using the

OmicShare Platform with sample clustering.

2.7. MMP activity determined by in situ zymography and gelatin zymography

The fluorescein-conjugated gelatin substrate, DQ gelatin (D12054, Invitrogen, USA), was prepared according to the manufacturer's instructions. The substrates were then added to the frozen sections (7 μm) and incubated at 37 °C for 18 h before being inspected using a fluorescent microscope (LSM800, Zeiss, Germany). ImageJ (National Institutes of Health, USA) was used to determine the intensity of the fluorescence, and the results were presented as a percentage of the fluorescence area across each cross section. Gelatin zymography was used to measure the MMP activity of cells that were cultured in FBS-free conditioned medium. The MMP activity of RASMCs cultured in FBS-free conditioned medium was assessed with gelatin zymography. The conditioned medium of RASMCs was collected and electrophoreted in a polyacrylamide gel, adding 0.1% (*w*/*v*) gelatin. The gels were then washed, incubated, and stained as described previously[44].

2.8. Immunohistochemistry and immunofluorescence

Sections embedded in paraffin were deparaffinized and rehydrated in accordance with earlier research[45]. Sections were incubated in Antigen Unmasking Solution (H-3301, Vector Laboratories, USA) at 98 °C for 10 min in order to retrieve the antigen. The slices were then blocked and treated with primary antibodies indicated in Table S1 for a whole night at 4 °C. On the following day, after removing the primary antibody, immunohistochemical staining was carried out using the 3,3′-diaminobenzidine peroxidase substrate kit (SK-4100, Vector Laboratories, USA), or for immunofluorescence staining, corresponding fluorescent secondary antibodies were employed. Cell immunofluorescence staining was performed as previously described[39]. All images were captured with either a Zeiss confocal microscope or an upright microscope (BX53, Olympus Corporation, Japan), and quantitative analysis was conducted using ImageJ.

2.9. Antioxidant capability measurement

After being exposed to various treatments, RASMCs were incubated with 5 μmol/L DHE (D1008, UElandy Inc., China) for 60 min at 37 °C. After that, cells were cleaned with PBS to get rid of any unreacted DHE, and a fluorescence microscope was used to

observe the existence of ROS. Following trypsin digestion at a concentration of 0.05%, the cells were suspended in cold PBS. A flow cytometer (BD FACSCanto, Becton, Dickinson and Company, USA) was used to count and evaluate ROS-positive cells, and FlowJo software (Becton, Dickinson and Company, USA) was used to analyze the data. Frozen aortic tissue slices were stained with 5 μmol/L DHE for 60 min at 37 °C in the dark and then photographed by fluorescence microscopy. Superoxide dismutase (SOD) and malondialdehyde (MDA) levels in treated RASMCs and Ang II-induced murine plasma were measured using the Total Superoxide Dismutase Assay Kit with NBT (S0109, Beyotime Institute of Biotechnology, China) and the Lipid Peroxidation MDA Assay Kit (S0131S, Beyotime Institute of Biotechnology, China) according to the manufacturer's instructions.

2.10. Nuclear and cytoplasmic protein extraction

At collection time points, RASMCs and MASMCs were washed three times with cold PBS after removing the culture medium. Nuclear and cytoplasmic protein lysates were extracted from SMCs using the Nuclear and Cytoplasmic Protein Extraction Kit (P0027, Beyotime Institute of Biotechnology, China) following the manufacturer's instructions.

2.11. Cell viability assay

RASMCs were seeded overnight in 96-well plates at 8×10^3 cells per well, then incubated with varying DHM doses over 24 h. CCK-8 kits were applied to test cell viability as we previously described[46].

2.12. Western blot

Cells and tissues were homogenized in RIPA buffer (P0013B, Beyotime Institute of Biotechnology, China) with 1% protease inhibitor cocktail (P1008, Beyotime Institute of Biotechnology, China). Protein concentrations were determined using the BCA Protein Assay Kit (23225, ThermoScientific, USA), and equal amounts of denatured proteins were separated on 8%–12% SDS-PAGE, then transferred to 0.22 μm PVDF membranes (ISEQ00010, Merck Millipore, Germany). After blocking with 5% non-fat milk, membranes were incubated overnight at 4 °C with primary antibodies (Table S1), washed in Tris buffered saline with Tween 20, and incubated with appropriate secondary antibodies (511203 or 511103, Zen BioScience, China) for 1 h at room temperature. Following a final wash, protein bands were detected using the Tanon 5200

chemiluminescent imaging system (China).

2.13. Real-time quantitative PCR (RT-qPCR)

TRIzol reagent was applied to extract the RASMCs' and MASMCs' total RNA. To create first-strand cDNA, 1 μg of total RNA was utilized with the ReverTra AceTM qPCR RT Kit (FSQ-101, Toyobo Co., Ltd., Japan). Using the corresponding gene-specific primers mentioned in Supporting Information Table S2, RT-qPCR was carried out using a LightCycler® 480 real-time PCR system (Roche, Switzerland) using SYBR® Premix Ex Taq™ II (RR820A, Takara, Japan). With *Gapdh* as the internal control, the $2^{-\Delta\Delta Ct}$ technique was utilized to quantify the relative gene expression. The results were presented as fold change in comparison to the control groups.

2.14. Cellular thermal shift assay (CETSA)

RASMCs were treated with 20 μmol/L DHM or DMSO for 4 h and harvested in PBS with protease inhibitors. The protein lysates were divided into eight portions and heated for 5 min at different temperatures (from 37 to 72 °C) in a SimpliAmp™ Thermal Cycler (SimpliAmp, Thermo Fisher Scientific Inc., USA), then cooled for 3 min at room temperature. After two freeze-thaw cycles in liquid nitrogen and centrifugation at 12,000×*g* for 20 min, the samples were mixed with loading buffer, heated at 95 °C for 10 min, and analyzed by Western blot.

For the isothermal dose-response fingerprints (ITDRF)-CETSA experiment, DHM was administered to RASMCs in increasing doses from 0 to 102.4 μmol/L for 4 h. Cells were collected in PBS with protease inhibitors, heated for 3 min at 55 °C, and cooled for 3 min at room temperature. After protein lysis, heat-treated samples were centrifuged at 12,000×*g* for 20 min at 4 °C. HO-1 levels were then assessed by Western blot.

2.15. Drug affinity responsive target stability (DARTS)

The RASMCs were rinsed twice with PBS and subsequently lysed using RIPA solution. Afterwards, the cell lysate that was obtained and divided evenly into individual tubes and then incubated at room temperature for 1 h with either DMSO or different concentrations of DHM. The samples underwent proteolysis using 20 μg/mL Pronase E (HY-114158A, MedChem Express, USA) for 20 min at room temperature. The reactions were halted by the addition of protein loading solution and prepared for

further analysis.

2.16. Chromatin immunoprecipitation assay (ChIP)

The ChIP procedure was done on 1×10^6 cross-linked MASMCs, and sonication was used to break up the DNA into pieces of 200 to 1000 base pairs[33]. The antibody–antigen complexes immunoprecipitated with antibodies against HIF-1α (36169, Cell Signaling Technology, USA) or IgG (3900S, Cell Signaling Technology, USA) were captured using Protein A/G Magnetic Beads (HY-K0202A, MedChem Express, USA). The ChIP signals were standardized to represent the percentage of input. Previous work has identified the primer sequences[47], which are available in Supporting Information Table S3.

2.17. Co-immunoprecipitation (Co-IP)

In the experiment investigating the impact of DHM on HO-1 ubiquitination in RASMCs, the cells were exposed to either DMSO or a concentration of 20 μmol/L DHM for a duration of 24 h. Before 12 h of cell collection, 20 μmol/L of MG132 was added to the cells to inhibit protein ubiquitination degradation. Co-IP was conducted using methods from prior investigation[48]. Briefly, cells were lysed in 100 μL of NETN buffer (62.5 mmol/L Tris-HCl (pH 6.8), 2% SDS, 10% glycerol, 20 mmol/L NEM, and 1 mmol/L iodoacetamide), boiled for 15 min, diluted to 400 μL with NETN buffer containing protease inhibitors, 20 mmol/L NEM, and 1 mmol/L iodoacetamide, and ultrasound broke up cells on ice. Centrifuged to remove cell debris, and protein concentration was determined by BCA. Cell extracts were subjected to 40 μg of cell lysate, which was taken as an input and stored at –20 °C for later use. The remaining cell lysate was mixed with HO-1 antibody and Protein A/G Magnetic Beads and incubated overnight in a 4-degree shaker. After incubation, the beads were cleaned with NETN buffer four times. Finally, 40 μL of 2× loading buffer was added and boiled at 95 °C for 5 min for Western blot verification.

2.18. His-labeled HO-1WT protein and HO-1K243R protein purification

The *HMOX1* gene was amplified using the KOD-Neo-Plus kit (KOD-401, TOYOBO, Japan) and subsequently extracted and purified with the agar-gel DNA extraction kit (D1200, Solarbio, China). The pET28a plasmid and *HMOX1* gene were double-digested and ligated using T4 DNA ligase (EL0014, ThermoScientific, USA) to

construct a His-tagged HO-1^{WT} recombinant plasmid. The endonuclease enzymes utilized in this study were NdeI (ER0582, Thermo Scientific, USA) and BamHI (ER0051, Thermo Scientific, USA), respectively. The Fast Mutagenesis System (FM111-02, Transgen Biotech, China) was used to make the HO-1^{K243R} plasmid, with the HO-1^{WT} plasmid serving as a template. The primers utilized for constructing plasmids can be found in Supporting Information Table S4. The His-tagged HO-1^{WT} and HO-1^{K243R} plasmids were transfected into *Escherichia coli* BL21 (DE3) (CD601-01, TransGen Biotech, China) and expressed with 0.5 mmol/L Isopropyl *β*-D-thiogalactoside at 25 °C for 16 h. The proteins were isolated using Ni-NTA His-Tag Purification Agarose (HY-K0210, MedChem Express, USA), following the purification protocols as reported previously[49].

2.19. Isothermal titration calorimetry (ITC)

The ITC assay was conducted utilizing a MicroCal PEAQ-ITC instrument (Malvern, USA) at a temperature of 25 °C. Before the experiment began, the protein samples were dialyzed in a buffer solution that contained 20 mmol/L Tris-HCl (pH 7.5) and 200 mmol/L NaCl. The DHM compound was thoroughly dissolved in the same buffer solution. After cleaning the instrument's cell and syringe, DHM was placed in the sample cell, and the HO-1 protein was placed in the syringe. The stirred calorimeter cell, which originally contained around 5 μmol/L of DHM, was successively injected with HO-1 protein at a concentration of approximately 50 μmol/L. Nineteen times, this injection procedure was carried out. In the end, a one-binding site model was used to fit the integrated corrected and concentration-normalized peak regions of the raw data in MicroCal PEAQ-ITC Analysis Software.

2.20. Molecular docking

The PubChem database (https://pubchem.ncbi.nlm.nih.gov/) was used to determine the structure of DHM (Compound CID: 161557). The HO-1 protein crystal structure (AF-P09601-F1) was obtained from the AlphaFold Protein Structure Database (https://alphafold.com/). Molecular Operating Environment 2015 (MOE 2015, Chemical Computing Group ULC, Canada) was used to create a molecular docking model of DHM with HO-1. Following the completion of molecular docking, the types of interactions between the docked protein and the ligand were investigated.

2.21. High-performance liquid chromatography (HPLC) analysis

After oral administration of DHM, blood samples were collected *via* orbital blood extraction into K_2-EDTA anticoagulant tubes (EDTA-K_2, G-CLONE, China) at the 1-h mark. The samples were centrifuged at 2000×*g* for 10 min at 4 °C within 1 h of collection, and all samples were stored at –80 °C. Prior to HPLC analysis, the samples were conditioned to room temperature. A 150-μL aliquot of plasma was mixed with 300-μL of methanol containing 2% acetic acid (*v*/*v*). In the blank control group, DHM was added at concentrations of 0, 0.1, 1, 10, and 100 μg/mL. These mixtures were swirled for 3 min to precipitate endogenous proteins in the plasma and then centrifuged at 10,000×*g* for 10 min at 4 °C. The supernatant was transferred to a new centrifuge tube and dried at 35 °C under a nitrogen stream. The residue was then dissolved in 250 μL of methanol, and 100 μL was injected into the HPLC column for analysis. DHM was detected using a Shimadzu HPLC system (LC-2050C 3D, Shimadzu, Japan) with an ultraviolet detector. The ZORBAXSB-C18 column (150 mm × 4.6 mm, 5 μm) was utilized for chromatographic separation, with 1 mL/min mobile phase pumping. The first mobile phase was 74% A (water with 0.1% phosphate) and 26% B (methanol). The gradient elution procedure was 26% to 98% B from 0–15 min and 98% B from 15 to 32 min. The temperatures of the autosampler and column were set at 15 and 30 °C, respectively. The detection wavelength was 292 nm.

2.22. Data and statistical analysis

GraphPad Prism version 9.4 (GraphPad Software, San Diego, CA, USA) was used to conduct the statistical analyses. The data were represented as the means ± standard error of mean (SEM) unless otherwise stated. The normality and equal variance of all the data were examined. Student's *t*-test was employed to compare two groups if the data passed those checks. One-way ANOVA or two-way ANOVA followed by Bonferroni's *post hoc* tests was employed for comparisons involving more than two groups. If the data failed those tests, Mann–Whitney was used to compare two groups, Kruskal–Wallis was used to compare groups of more than two, and Benjamini, Krieger, and Yekutieli's two stage step-up approach was applied. The occurrence of AAA was examined using the Fisher exact test. The Kaplan–Meier method was utilized to generate survival curves for mice, allowing for an examination of their survival rates. The disparities between the survival rates were subsequently assessed through the log-rank (Mantel-Cox) test. Statistical significance was defined as a *P*-value less than 0.05.

3. Results

3.1. DHM decreases the incidence of AAA and preserves the structural integrity of the aortic wall in the Ang II-induced murine AAA model

ApoE$^{-/-}$ mice combined with Ang II infusion are clinically relevant and the most commonly used murine AAA model. To investigate the effect of DHM on AAA initiation and progression *in vivo*, ApoE$^{-/-}$ mice were treated daily with vehicle or either low or high doses of DHM on the day of Ang II infusion (Fig. 1A). By the 28th day following mini-pump implantation, a substantial number of mice in the Model (Ang II infusion plus vehicle) group exhibited noticeable AAA in contrast to the Saline group, whereas DHM administration successfully hindered AAA formation in a dose-dependent manner (Fig. 1B). We establish the definition of an AAA as an abdominal aorta with a diameter exceeding 1.5 times the average diameter of the Saline group. After Ang II infusion, a high dosage of DHM exhibited a significant reduction in both AAA incidence (20.00%) and abdominal aorta dilation (1.19 ± 0.07 mm) as compared to the Model group (AAA incidence of 73.33% and maximal diameter of 1.91 ± 0.18 mm), as depicted in Fig. 1C and D. In addition, we observed that the administration of high doses of DHM enhanced the survival rate in the murine AAA model (Supporting Information Fig. S1A). However, it did not appear to have an impact on the elevation of SBP induced by Ang II (Fig. S1B).

Insert Fig. 1

The destruction of the aortic wall and immune-mediated infiltration are critical for the development of AAA. To assess these pathological changes, we compared the structural integrity of the mouse aorta using H&E, VVG, and Masson's trichrome staining, as well as evaluated inflammatory responses and macrophage infiltration by performing immunohistochemistry for VCAM1 and CD68. A significant difference was noticed in the aortas of mice in the Model group. This group displayed distinct features, including thickening and remodeling of the aortic adventitia, fragmentation of elastin, and a decrease in collagen content within the medial layer (Fig. 1E). However, DHM treatment kept the structural integrity of the murine aorta, slowed down the breakdown of elastin, and raised the amount of collagen in the aortic media (Fig. 1E–G). Furthermore, DHM-treated mice showed a dose-dependently considerably smaller VCAM1- and CD68-positive region in the aorta wall in comparison with mice in the Model group (Fig. S1C). In addition to inflammatory responses, the increase of MMP expression and activity and the decrease in the contractile phenotype of SMCs

contribute to the pathogenesis of AAA. *In situ* zymography immunofluorescence staining showed higher MMP activities in the Model group than those of ApoE$^{-/-}$ mice in DHM-treated group (Fig. 1H and Fig. S1D). In addition, Western blots and immunohistochemistry illustrated that the levels of contractile phenotype markers *α*-SMA and CNN1 were drastically lower, and expression of MMP2 and MMP3 was significantly raised after Ang II infusion, of which the results were effectively reversed by high-dose DHM treatment (Fig. 1I–L). Finally, ELISA assays confirmed that the Model group of mice had an up-regulation of three crucial AAA-related cytokines (IL-1*β*, IL-6, and TNF-*α*); however, treatment with DHM effectively suppressed the rise of these cytokines (Fig. S1E–S1G). Taken together, these findings demonstrate that DHM inhibits the formation of AAA and preserves the structural integrity of the aortic wall in the Ang II-induced murine AAA model.

3.2. DHM promotes the activation of the HIF-1α/HO-1 pathway in SMCs

To acquire a more thorough knowledge of the role of DHM in AAA, we employed network pharmacology to study the anti-AAA effect of DHM and the underlying mechanisms. Initially, we established two separate target networks: the AAA-target network, comprising 2522 nodes with 94,150 connections, and the DHM-target network, which consisted of 424 nodes with 5737 connections (Fig. 2A). By merging these two networks, an overlapping network encompassing AAA- and DHM-related targets was formed, comprising 182 nodes and 2695 connections, with TTPA buried as a free node. To explore further key nodes in the overlapping network, we focused on the nodes whose degree values were 1.5 times or higher than the median value of 182 common nodes, forming a hithub network with 36 nodes. Within this focused network, five targets highlighted in red (MMP2[50], MMP9[51], CCL5[52], HMOX1[25], and HIF-1*α*[29]) are important in AAA, as they have been demonstrated to be closely associated with the development of AAA.

Insert Fig. 2

To comprehensively investigate the potential and underlying mechanisms of DHM in preventing AAA, we conducted an enrichment analysis on the 182 common targets, encompassing DO, KEGG, and GO. The DO analysis revealed that 7 out of the top 15 items were significantly associated with human vascular diseases (Fig. 2B), indicating DHM's potential in preventing and treating vascular diseases, including AAA. KEGG functional enrichment analysis revealed that the 182 intersection targets were notably

enriched in the "Lipid and atherosclerosis" and "Fluid shear stress and atherosclerosis" pathways, associated with atherosclerosis, a known AAA risk factor (Supporting Information Fig. S2A)[53]. Additionally, KEGG analysis showed that DHM is involved in the signaling pathway of HIF-1, one of the transcription factors that control *HMOX1* transcription[19,54]. Delving into the GO analysis results, we observed that DHM primarily enriched categories associated with immune response, oxidative stress, collagen synthesis, and the ECM (Fig. S2B). Given that inflammation, oxidative stress, and ECM degradation are key hallmarks of AAA, we predicted that DHM might act to prevent AAA formation by means of anti-inflammatory, antioxidant, and regulated ECM homeostasis. Within these mechanisms, HO-1 might emerge as a critical target for DHM, with HIF-1 serving as the transcription factor governing HO-1 expression.

To delve deeper into the potential role of HO-1 as a pivotal target of DHM in AAA prevention, we isolated and cultured the key AAA-associated cells (such as macrophages, endothelial cells, and SMCs). These cells were identified based on their morphology or by detecting specific cell markers, and then exposed to different doses of DHM. The Western blot results revealed that DHM elevated HO-1 expression in RBMDMs, RAECs, and RASMCs in a dose-dependent manner, with the most pronounced effect in SMCs, surpassing the impact on endothelial and macrophage cells by more than threefold (Fig. 2C). Following the isolation of MASMCs and the identification of their morphology and cell markers, we also observed that DHM treatment significantly increased HO-1 levels in MASMCs, which was consistent with the results observed in RASMCs (Fig. S2C). Remarkably, 20 μmol/L DHM substantially increased the HO-1 protein expression by ~10-fold in RASMCs (consistent with the results in MASMCs), which is much better than the effects seen with other traditional Chinese medicine monomers that have been reported to target the NRF2/HO-1 signaling pathway[55] (Fig. S2D). These observations highlight the potential importance of DHM-mediated remarkable effect on HO-1 expression in SMCs, prompting us to investigate the interaction between DHM and SMCs further.

To confirm our assumptions regarding the role of DHM in the HIF-1α/HO-1 signaling pathway in SMCs, we conducted RNA-seq on RASMCs treated with DHM. CCK8 assay confirmed RASMC activity remained unaffected under 300 μmol/L DHM (Fig. S2E), and dose-response results indicated 20 μmol/L as the optimal DHM concentration for enhancing HO-1 expression in RASMCs (Fig. S2F). Therefore, we pretreated the RASMCs with 20 μmol/L DHM before RNA-seq analysis to identify

differentially expressed genes in RASMC mRNA profiles. The volcano plot illustrated an upregulation of genes related to the HIF-1 signaling pathway in response to DHM, with *Hmox-1* displaying the most significant upregulation among all the genes (Fig. 2D). Significantly, the KEGG analysis of differentially expressed genes revealed that DHM had a pronounced impact on the HIF-1 signaling pathway, aligning with the outcomes from network pharmacology (Fig. 2E). Additionally, it was observed to influence pathways associated with inflammation, such as the TNF signaling pathway and cytokine–cytokine receptor interaction. In the GO enrichment analysis, it became evident that DHM exerted its influence on various aspects (Fig. 2F). Specifically, in the cellular component category, DHM affected the ECM and collagen. In terms of molecular function, it impacted the activity and binding of inflammatory factors, ECM binding, and collagen binding. As for the biological process category, DHM played a role in responses to ROS and inflammation. Taken together, these findings indicate that DHM plays a role in modulating SMC homeostasis, including SMC inflammation, oxidative stress and the ECM organization, which might be mechanistically associated with the HIF-1α/HO-1 signaling pathway.

Studies indicated that HIF-1α promoted elastin fiber formation[29], boosted tissue inhibitors of matrix metalloproteinases[30] to safeguard ECM integrity and against aortic aneurysms, regulated collagen synthesis[56,57], curbed mitochondrial oxidative metabolism to reduce ROS[58], and promoted HO-1 transcription[19,20,54,59]. Combined with these research results, we generated a heatmap including genes divided into heme and iron metabolism, mitochondrial oxidative metabolism, and ECM composition, proposing that DHM might exert its anti-AAA effects by modulating these genes through the HIF-1/HO-1 pathway, with HO-1 emerging as a pivotal target in this process (Fig. 2G). Some of the key genes were further verified by RT-qPCR in RASMCs (Fig. S2G). We also evaluated the expression and activation of NRF2, the primary transcription factor for HO-1, in DHM-treated RASMCs. Surprisingly, DHM affected neither NRF2 protein expression nor its downstream target genes in RASMCs (Fig. S2H and S2I). Furthermore, RT-qPCR results in MASMCs demonstrated that DHM effectively modulated the expression of *Hmox1* and HIF-1α signaling pathway-associated genes (such as *Binp3*, *Ldha*, *Eln*, and *Col12a1*) while having no impact on the expression of NRF2 signaling pathway-related genes (*Ftl1* and *Fth1*) (Fig. S2J). Thus, it appears that DHM promotes transcriptional upregulation of *Hmox1* in SMCs *via* HIF-1α rather than NRF2.

3.3. DHM orchestrates ECM, SMC phenotypes, inflammation, and ROS via activating HIF-1α/HO-1 both in vivo and in vitro

To further examine the role of DHM in regulating SMC homeostasis and the development of AAA, we simulated an *in vitro* AAA model using TNF-*α* with RASMCs or MASMCs to assess the impact of DHM. TNF-*α* has been commonly employed as a stimulant to replicate AAA[6,37,60], a cytokine that has been observed to significantly increase in both human and murine AAA[61,62]. The Western blot results revealed that DHM enhanced elastin expression in a dose-dependent manner while thwarting the reduction of TNF-*α*-induced SMC contractile phenotype both in RASMCs and MASMCs (Fig. 3A and Supporting Information Fig. S3A). Moreover, DHM effectively suppressed the expression of MMP2, MMP3, and MMP9 at both the protein (Fig. 3B and Fig. S3B) and mRNA levels (Fig. 3C), while also inhibiting the activities of MMPs, as demonstrated by the gelatin zymogram result (Fig. S3C). Concurrently, we employed a broad-spectrum MMP inhibitor (DOXY) as a positive control in the AAA treatment[63]. Furthermore, RT-qPCR results demonstrated that DHM can downregulate the expression of inflammatory cytokines, including *Il1β*, *Il6*, and *Tnfα* (Fig. 3C), which is consistent with the data obtained from the ELISA assays (Fig. S1E–S1G). These findings suggest that DHM might uphold the composition of the SMC's ECM by promoting elastin synthesis and inhibiting MMP-mediated ECM degradation. Additionally, it appears to block SMC phenotypic transformation by reducing the expression of inflammatory factors. Aside from proteases and cytokines, oxygen-derived free radicals are pivotal in driving SMC phenotype changes and ECM degradation, key factors in AAA development. We further investigated the antioxidant capabilities of DHM using a kind of ROS probe, DHE. Both flow cytometry and immunofluorescence imaging showed that TNF-*α* or Ang II significantly increased ROS levels in the RASMCs or aortic media *in vivo*, whereas DHM effectively reduced this elevation (Fig. 3D and E). In line with these results, SOD levels were shown to decrease while MDA contents were increased in both serum from Ang II-treated AAA mice and TNF-*α*-exposed RASMCs, an effect that was prevented step by step with increasing concentrations of DHM (Fig. S3D). These findings indicate that DHM plays a critical role in SMC contractile phenotype, ECM composition, inflammation, and ROS production.

Insert Fig. 3

Based on the findings of network pharmacology and RNA-seq, we further studied

the effects of DHM on HIF-1α/HO-1 to clarify the regulatory mechanisms of DHM in AAA. Western blot and immunohistochemistry revealed that HIF-1α expression remained unaltered in the aortic media of DHM-treated AAA mice, but DHM treatment resulted in a significant increase in the expression of HIF-1α target proteins HO-1 and elastin (Fig. 3F and G). The RNA-seq results suggest that DHM stimulates the activation of HIF-1 signaling pathway. As a result, we propose that DHM may enhance HIF-1α transport into the nucleus rather than simply raising its protein levels to regulate HIF-1α signaling pathway. To test our hypothesis, additional analysis was conducted by separating the cytoplasmic and nuclear components of RASMCs and MASMCs treated with DMSO, DHM, DMSO + TNF-α, or DHM + TNF-α. The results revealed a notable increase in nuclear HIF-1α levels with DHM treatment, accompanied by a corresponding reduction of HIF-1α in the cytoplasm (Fig. 3H and Fig. S3E). Immunofluorescence results also provided evidence of DHM's role in facilitating the nuclear translocation of HIF-1α, which led to a significant rise in HO-1 levels in SMCs and murine aortic media (Fig. 3I and Fig. S3E–S3I). These findings further indicate that DHM promotes the nuclear translocation of HIF-1α. Western blot analysis of DHM-treated RASMCs demonstrated that HIF-1α protein levels remained constant, while the content of HO-1 increased as the DHM concentration was raised (Fig. 3J). The RT-qPCR results confirmed the elevation of *Hmox1* in a dose-dependent manner (Fig. 3L). However, according to the RNA-seq findings, DHM did not affect the levels of *Hif1a* mRNA (Fig. 3K). Moreover, immunofluorescence results further supported the notion that DHM effectively amplified HO-1 expression and counteracted the decrease in contractile markers within SMCs both in RASMCs and MASMCs (Fig. S3J and S3K). Importantly, HIF-1α inhibitor CAY10585 (LW 6), but not NRF2 inhibitor ML385, partly reversed DHM-induced protein expression of HO-1 (Fig. 3M). Additionally, ChIP-qPCR analysis revealed that DHM stimulated the binding of HIF-1α to the promoter region of *Hmox1* (Fig. 3N and O). These findings suggest that the significant increase in HO-1 protein induced by DHM is at least partially dependent on the nuclear-translocating HIF-1α binding to the *Hmox1* promoter. Overall, these findings suggest that DHM regulates the HIF-1/HO-1 signaling pathway through the facilitation of HIF-1α's nuclear translocation in SMCs.

3.4. DHM impedes the degradation of HO-1 by forming a binding interaction with Lys243 on the HO-1 protein

Since DHM-induced HO-1 protein expression could only be partly reversed by HIF-1α inhibitor, we posited that there may be other mechanisms except for HIF-1α-mediated transcriptional regulation. Consequently, we employed CHx to inhibit protein synthesis to investigate the impact of DHM on the protein degradation of HO-1 in RASMCs. Our results indicated that when protein synthesis is inhibited, DHM significantly suppressed the degradation of HO-1 (Fig. 4A). At 12 h after CHx treatment, the group that was given DHM had a level of HO-1 protein that was 67.3 ± 9.5%, which was about twice as high as the level seen in the DMSO-treated group, which was 36.3 ± 4.5%. Thus, DHM modulates both the transcription and degradation of HO-1 in SMCs, leading to the massive accumulation of HO-1 protein.

To gain further structural insight into the mechanism by which DHM influences the degradation of HO-1, we performed a CETSA, DARTS, molecular docking analysis, ITC, and Co-IP to infer whether there is a direct interaction between DHM and HO-1. CETSA experiments conducted with RASMCs revealed that DHM significantly enhanced the thermal stability of HO-1, resulting in an upregulation of approximately 10.43 °C in the T_{m50} value (Fig. 4B). The ITDRF-CETSA study further confirmed DHM's dose-dependent binding and significant stabilization of the HO-1 protein (IC_{50} = 2.5 μmol/L, Fig. 4C). Similarly, the DARTS experiment demonstrated that the degradation of HO-1 protein by protease E was reduced in the presence of DHM (Fig. 4D). We employed MOE software to predict the binding of DHM and HO-1 molecules and discovered an interaction (binding energy: –7.4 kcal/mol) between DHM and Lys243 of HO-1 (Fig. 4E). Simultaneously, prior mass spectrometric data from PhosphoSitePlus (https://www.phosphosite.org) indicated that Lys243 is the probable ubiquitination site for HO-1. As an additional verification of the binding between DHM and Lys243 of HO-1, we constructed plasmids for HO-1^{WT} and HO-1^{K243R} and purified both of the two proteins (Supporting Information Fig. S4). These plasmids were introduced into *Escherichia coli* BL21 (DE3) for culture to induce the expression of the respective proteins, which were purified using Ni-NTA His-Tag Purification Agarose (Fig. 4F). Subsequently, we conducted ITC experiments to investigate the affinity between these two proteins and DHM. The results indicated that DHM exhibited a higher affinity for purified HO-1^{WT}, with a dissociation constant (K_D) value of 368 ± 182 nmol/L (Fig. 4G). However, when the lysine at position 243 of HO-1 was mutated to arginine, the interaction between DHM and HO-1 was disrupted (Fig. 4H). In addition, the binding capacity between HO-1^{K243R} mutated protein and DHM was

evaluated by CETSA and showed a notable decline in thermal stability of HO-1^{K243R} protein with DHM compared to HO-1^{WT} protein (Fig. 4I). Under basal circumstances, the HO-1 protein undergoes ubiquitination at the Lys243 site and undergoes degradation[64]. Therefore, we hypothesized that DHM may directly interact with the Lys243 residue in HO-1, thereby obstructing the binding between HO-1 and ubiquitin, and Co-IP was adopted to verify this hypothesis. We used the Co-IP experiment to investigate whether the presence or absence of DHM influenced the interaction between HO-1 and ubiquitin, and found that DHM impeded this interaction (Fig. 4J). Taken together, these results imply that DHM might directly bind to SMC Lys243 in HO-1 to hinder the binding of HO-1 and ubiquitin, thereby impeding the degradation of HO-1.

Insert Fig. 4

3.5. Competitive inhibition of HO-1 reverses the protective effect of DHM on AAA in vitro

Having shown that DHM significantly upregulates HO-1 expression and attenuates AAA formation, we next asked whether HO-1 induction underlies DHM-mediated protective effects on AAA. We employed ZnPPIX as a competitive inhibitor of HO-1 and subsequently investigated the effects of DHM on ECM composition, cellular phenotypic transition, inflammation and oxidative stress in TNF-*α*-treated RASMCs. DHM treatment recovered TNF-*α*-induced downregulation of the protein expression of elastin, *α*-SMA, SM22*α*, and CNN1 in RASMCs. However, these effects were completely abolished when HO-1 activity was restricted by ZnPPIX treatment (Fig. 5A). Additionally, Western blot and qPCR analyses showed that ZnPPIX interfered with DHM's ability to reduce the expression of MMPs and inflammatory factors in DHM-treated RASMCs (Fig. 5B and C). Furthermore, ZnPPIX also reversed DHM-mediated antioxidant capabilities, as evidenced by the detection of ROS, SOD, and MDA levels (Fig. 5D–G). Collectively, these findings suggest that DHM exerts its protective effect on VSMC homeostasis *via* activating HO-1 *in vitro*.

Insert Fig. 5

3.6. SMC-specific Hmox1 knockdown abolishes the protective effect of DHM in Ang II-induced murine AAA model in vivo

To examine the potential role of HO-1 in SMCs as a crucial target for DHM in the regulation of AAA *in vivo*, we generated an VSMC-specific *Hmox1* shRNA (sh*Hmox1*)

AAV serotype 2 vector. This vector included a combination of promoters unique to VMSCs (SM22α promoter), together with GFP and a mouse sh*Hmox1* sequence to suppress the expression of *Hmox1* (AAV-sh*Hmox1*) (Fig. 6A). The control virus (AAV-sh*Ctrl*) and AAV-sh*Hmox1* were administered to mice by intravenous injection *via* the tail vein, respectively. During the second week following injection, Western blot experiments were performed using the brain, aortic media, liver, kidney, and lung of mice. The results indicated that the expression of the HO-1 protein in the brain, liver, kidney, and lung remained unaffected by the two AAV2 viruses. However, the introduction of AAV-sh*Hmox1* significantly disrupted the expression of HO-1 in the medial VSMCs of the aorta (Fig. 6B and Supporting Information Fig. S5A and S5B). The fluorescence imaging analysis of various tissue organs demonstrated that the AAV exhibited a specific infection of the aorta (Fig. 6C). After confirming the efficacy of AAV, we administered the AAV2 virus to mice and then established a mouse AAA model induced by Ang II using the previously described protocol (Fig. 6D). We observed that DHM effectively inhibited the formation of AAA in Ang II-infused ApoE$^{-/-}$ mice. Notably, this inhibitory effect was significantly attenuated when HO-1 expression was suppressed in VSMCs, as evidenced by the augmented incidence of AAA and increased maximum diameter of the abdominal aorta (Fig. 6E–G). Moreover, a marked elevation in survival rates was noted following high-dose DHM treatment in mice with AAA, an effect that was abrogated in the context of HO-1 knockdown (Fig. S5C). Blood pressure assessments across the experimental groups were measured, and we found no noticeable changes in SBP in these mice (Fig. S5D). Further immunofluorescence studies revealed that DHM administration substantially upregulated HO-1 expression in SMCs. This upregulation was impeded by employing AAV-sh*Hmox1*, which concurrently led to a reduction in α-SMA protein levels (Fig. 6H). Immunohistochemical analyses corroborated these findings, demonstrating that AAV-mediated sh*Hmox1* effectively inhibited DHM-induced HO-1 overexpression in SMCs (Fig. 6I). Histological assessments using H&E, VVG, and Masson's trichrome staining illustrated a clear link between HO-1 deficiency and the reduced efficacy of DHM therapy. This was manifested by notable adventitial thickening, enhanced elastin fragmentation, and a significant decrease in collagen content within the medial layer of the aorta (Figs. 6J, 7A and B). Additionally, immunohistochemical and Western blot analyses revealed that HO-1 knockdown in SMCs offset the therapeutic effect of DHM by increasing inflammation, promoting SMC phenotypic changes, and elevating MMP

levels, despite the fact that DHM treatment could improve AAA by increasing HO-1 and elastin levels, underscoring the potential of HO-1 as a pivotal therapeutic target in AAA treatment (Fig. 7C–E and Fig. S5E). The HO-1 knockdown was also associated with augmented MMP activity, increased oxidative stress and elevated cytokines (IL-1β, IL-6, and TNF-α) in DHM-treated AAA mice (Fig. 7F–H and Fig. S5F–S5H), further highlighting its integral role in AAA pathogenesis. From these findings, we conclude that HO-1 upregulation in SMCs contributes to the protective effects of DHM on vascular homeostasis and AAA formation *in vivo*.

Insert Figs. 6&7

4. Discussion

The pressing need to identify effective pharmacological strategies for prevention, suppression, or reversal is underscored by the high rupture risk associated with AAA, a critical vascular condition. In this study, we have shed light on the potential of DHM, a bioactive flavonoid abundantly found in *A. grossedentata*, to curb the expansion of AAA in an Ang II-induced murine model. This effect of DHM is mediated by the activation of the HIF-1α/HO-1 signaling axis and the inhibition of HO-1 ubiquitination degradation. The former mechanism is associated with DHM promoting the nuclear translocation of HIF-1α, thereby stimulating the binding of HIF-1α to the promoter region of *Hmox1*. The latter mechanism involves DHM obstructing the interaction between HO-1 and ubiquitin, perhaps by attaching to HO-1 at Lys243[64], a critical location for ubiquitination, thereby competitively preventing ubiquitin from binding to HO-1. This dual mechanism underscores a novel therapeutic approach that targets both the transcription and degradation of HO-1 in AAA therapy.

Despite the exploration of various pharmacological agents like DOXY, ACE inhibitors, and statins for the prevention of AAA, clinical trials have consistently yielded negative outcomes[65-67]. In contrast, our study harnesses a widely recognized AAA model[68-70] to elucidate the inhibitory effects of DHM on AAA development. Utilizing ApoE$^{-/-}$ mice, known to induce hyperlipidemia, we simulated the core characteristics of human AAA through Ang II infusion, concomitant with hyperlipidemia. Our results suggested a significant decrease in AAA incidence (from 73.33% to 20.00%) following DHM treatment, thereby establishing DHM as a promising new agent in AAA management. Crucially, the therapeutic efficacy of DHM was almost entirely negated when HO-1 expression was knocked down in SMCs, with

AAA incidence escalating from 26.67% to 73.33%. Our *in vitro* findings indicated that MMPs and inflammatory cytokines notably increased due to acute oxidative stress post-TNF-*α* stimulation. DHM treatment, however, elevated both HO-1 protein and mRNA levels, and its protective effect against RASMC inflammation intensified with HO-1 upregulation. The modulation of *Mmp2*, *Mmp3*, *Mmp9*, *Il1β*, *Il6*, and *Tnfα* gene expression by DHM was almost negated upon HO-1 inhibition. Furthermore, DHM treatment safeguarded the aortas from inflammation and oxidative damage, thereby preserving their structural integrity. Due to the fact that DHM promoted the HIF-1*α*/HO-1 signaling axis, the rate of synthesis of elastic fibers increased, and the rate of degeneration of elastic fibers was restrained. We believe that DHM inhibited AAA mainly by maintaining ECM homeostasis by promoting the synthesis of elastic fibers and inhibiting the degeneration of elastic fibers. Notably, we found a disproportionate increase in HO-1 protein levels compared to mRNA following DHM treatment. Inhibition of protein synthesis in RASMCs for 6 h significantly postponed HO-1 degradation with DHM treatment. Additionally, DHM enhanced HO-1 stability and interacted with Lys243 to inhibit ubiquitination at this site.

HO-1, known for its antioxidative effects, is a stress-inducible, intracellular enzyme crucial in various biological processes, including oxidative stress, inflammation, apoptosis, and cell proliferation[20]. All of these processes are relevant to the pathogenesis of AAA[37,71-73]. In the initiation and progression of AAA, the expression of HO-1 is upregulated in both murine[25,74] and human models[24,27], conferring a critical role in AAA formation. It has been demonstrated that HO-1 deficiency in mice leads to increased susceptibility to AAA, characterized by severe elastin degradation and SMC loss[25,75]. In the context of AAA, the modulation of HO-1 presents a complex scenario extending beyond the traditional NRF2 pathway. Typically, HO-1 is regulated by the NRF2 transcription factor; however, a recent study[76] revealing NRF2-independent upregulation of HO-1 following Simvastatin treatment in AAA patients suggests the presence of alternative regulatory mechanisms. This insight opens the possibility of exploring NRF2-independent *HMOX1* modulation as a new strategy for AAA treatment. Besides NRF2, HIF-1*α* not only serves as a transcription factor for *HMOX1*, but its deletion has been shown to exacerbate AAA[29]. In this study, we have uniquely demonstrated that DHM treatment distinctly upregulates HO-1 protein levels *via* HIF-1*α* regulation, bypassing the NFR2 pathway. This groundbreaking finding uncovered an innovative therapeutic target within the HIF-1*α*/HO-1 signaling axis for

AAA treatment. What's more, additional natural substances that can markedly enhance HO-1 expression may likewise have anti-AAA properties. We recently reported that ginkgolide B and *Citri reticulatae pericarpium* can activate the NRF2/HO-1 pathway[77,78]. The potential of these natural chemicals to suppress AAA through the upregulation of HO-1 warrants further investigation.

The current understanding of HO-1 has gone beyond the conventional realm of transcription factor activity, delving into the realm of protein stability. Accumulating evidence indicates that the modulation of HO-1 encompasses not only the influence of transcription factors on its expression level and activity but also the processes of ubiquitination and proteasome-mediated degradation[79,80]. For example, recent research[80] has pinpointed the 14-3-3ζ protein as a novel interacting partner of HO-1. This interaction is crucial as it impedes the ubiquitination and proteasome-mediated degradation of HO-1, thus enhancing its stability. These insights underscore an alternative approach to modulating HO-1 levels through its degradation pathway. Intriguingly, our work revealed that DHM hindered the degradation of HO-1, potentially by disrupting ubiquitin's binding to HO-1 at Lys243, which promoted protein accumulation. Consistent with our findings, Song et al. demonstrated that HO-1 undergoes ubiquitination at Lys243 under resting conditions, leading to its degradation[80]. In addition to the canonical role of ubiquitin in tagging proteins for proteasomal degradation, a recent study[81] has identified the midnolin-proteasome pathway as a mechanism for ubiquitination-independent protein degradation. The implications of this pathway in the regulation of HO-1 degradation and the potential influence of DHM on this process present intriguing directions for future research. Unraveling whether DHM can modulate this novel degradation pathway could offer valuable insights into the complex regulation of HO-1 and its therapeutic potential.

Unfortunately, a significant obstacle to using DHM as a therapeutic treatment is its limited capacity to be absorbed orally, which is a widespread problem among other flavonoids (such as naringenin[82] and quercetin[83]). In our study, despite administering a high dosage of 250 mg/kg DHM daily through gavage for 4 consecutive weeks, the plasma concentration in mice only reached 14.88 ± 6.833 μmol/L (Supporting Information Fig. S6). This concentration barely aligns with the effective range used in our *in vitro* experiments (1–20 μmol/L), underscoring the need for large doses to achieve relatively effective plasma concentration. Similarly, clinical studies have administered up to 940 mg of DHM per day to improve glycemic control[84], further

emphasizing the need to enhance DHM's bioavailability to make it more viable for therapeutic use. Researchers have investigated various approaches to enhance the bioavailability of DHM[85]. Methods such as cyclodextrin inclusion complex[86] and nanoencapsulation[87] have shown potential for enhancing the absorption and stability of DHM, which might possibly lead to a decrease in the necessary dose for therapeutic effectiveness. These sophisticated delivery methods have the potential to enhance the solubility, permeability, and bio-distribution of DHM, thereby increasing its efficacy at reduced dosages. Interestingly, hydroxypropyl-beta-cyclodextrin (HP-β-CD) has been identified not only as a delivery method to enhance the bioavailability of DHM but also as a potential treatment for AAA[37]. This dual functionality raises the question of whether using HP-β-CD to enhance the solubility of DHM could provide a synergistic effect in the treatment of AAA. Combining DHM with HP-β-CD might optimize therapeutic outcomes by leveraging the benefits of both compounds. Nevertheless, these delivery methods have not yet been used in the manufacturing and sales processes. We anticipate that this work will encourage the development of techniques to improve the bioavailability of DHM. Further research should focus on optimizing these delivery methods and assessing their effectiveness in clinical settings. Enhancing the bioavailability of DHM may optimize its therapeutic efficacy, possibly providing a viable therapy alternative for disorders such as AAA.

5. Conclusions

To summarize, our study showed that DHM protected against AAA formation by reducing VSMC inflammation and oxidative stress, blocking MMP expression and activity, promoting elastin production, and preserving VSMC contractile phenotype through transcriptional activation of HIF-1α-dependent HO-1 mRNA expression and competitive impedance of HO-1 protein degradation. Our findings interpret the mechanistic insight of DHM in alleviating AAA and paving the way for further research into the VSMC HIF-1α/HO-1 axis as a novel pathway for AAA therapy.

Acknowledgments

This work is supported by National Natural Science Foundation of China (Nos. 82270500, 82203304 and 81870324) and Guangdong Basic and Applied Basic Research Foundation (No. 2024B1515020113, China).

Author contributions

Weile Ye: Investigation, Formal analysis, Writing - Original Draft. Pinglian Yang: Investigation, Formal analysis. Mei Jin: Investigation, Formal analysis. Jiami Zou: Investigation. Zhihua Zheng: Investigation. Yuanyuan Li: Investigation. Dongmei Zhang: Writing - Review & Editing. Wencai Ye: Writing - Review & Editing. Zunnan Huang: Conceptualization, Supervision, Writing - Review & Editing. Jiaojiao Wang: Conceptualization, Funding acquisition, Supervision, Writing - Review & Editing. Zhiping Liu: Conceptualization, Funding acquisition, Supervision, Project administration, Writing - Review & Editing.

Conflicts of interest

The authors declare no conflicts of interest.

Reference

1 Golledge J, Thanigaimani S, Powell JT, Tsao PS. Pathogenesis and management of abdominal aortic aneurysm. *Eur Heart J* 2023;**44**:2682-97.

2 Obel LM, Diederichsen AC, Steffensen FH, Frost L, Lambrechtsen J, Busk M, et al. Population-based risk factors for ascending, arch, descending, and abdominal aortic dilations for 60–74-year-old individuals. *J Am Coll Cardiol* 2021;**78**:201-11.

3 Golledge J. Abdominal aortic aneurysm: update on pathogenesis and medical treatments. *Nat Rev Cardiol* 2019;**16**:225-42.

4 Zhang W, Zhao J, Deng L, Ishimwe N, Pauli J, Wu W, et al. INKILN is a novel long noncoding RNA promoting vascular smooth muscle inflammation *via* scaffolding MKL1 and USP10. *Circulation* 2023;**148**:47-67.

5 Jana S, Hu M, Shen M, Kassiri Z. Extracellular matrix, regional heterogeneity of the aorta, and aortic aneurysm. *Exp Mol Med* 2019;**51**:1-15.

6 Zhao G, Zhao Y, Lu H, Chang Z, Liu H, Wang H, et al. BAF60c prevents abdominal aortic aneurysm formation through epigenetic control of vascular smooth muscle cell homeostasis. *J Clin Invest* 2022;**132**:e158309.

7 Wei L, Bu X, Wang X, Liu J, Ma A, Wang T. Global burden of aortic aneurysm and attributable risk factors from 1990 to 2017. *Glob Heart* 2021;**16**:35.

8 Bulder RMA, Talvitie M, Bastiaannet E, Hamming JF, Hultgren R, Lindeman JHN. Long-term prognosis after elective abdominal aortic aneurysm repair is

poor in women and men: the challenges remain. *Ann Surg* 2020;**272**:773-8.

9 Zhang Q, Zhao Y, Zhang M, Zhang Y, Ji H, Shen L. Recent advances in research on vine tea, a potential and functional herbal tea with dihydromyricetin and myricetin as major bioactive compounds. *J Pharm Anal* 2021;**11**:555-63.

10 Zhang J, Chen Y, Luo H, Sun L, Xu M, Yu J, et al. Recent update on the pharmacological effects and mechanisms of dihydromyricetin. *Front Pharmacol* 2018;**9**:1204.

11 Carneiro RCV, Ye L, Baek N, Teixeira GHA, O'Keefe SF. Vine tea (*Ampelopsis grossedentata*): a review of chemical composition, functional properties, and potential food applications. *J Funct Foods* 2021;**76**:104317.

12 Chen S, Zhao X, Wan J, Ran L, Qin Y, Wang X, et al. Dihydromyricetin improves glucose and lipid metabolism and exerts anti-inflammatory effects in nonalcoholic fatty liver disease: a randomized controlled trial. *Pharmacol Res* 2015;**99**:74-81.

13 Ye L, Wang H, Duncan SE, Eigel WN, O'Keefe SF. Antioxidant activities of Vine tea (*Ampelopsis grossedentata*) extract and its major component dihydromyricetin in soybean oil and cooked ground beef. *Food Chem* 2015;**172**:416-22.

14 Jiang B, Le L, Pan H, Hu K, Xu L, Xiao P. Dihydromyricetin ameliorates the oxidative stress response induced by methylglyoxal *via* the AMPK/GLUT4 signaling pathway in PC12 cells. *Brain Res Bull* 2014;**109**:117-26.

15 Hou XL, Tong Q, Wang WQ, Shi CY, Xiong W, Chen J, et al. Suppression of inflammatory responses by dihydromyricetin, a flavonoid from *Ampelopsis grossedentata*, *via* inhibiting the activation of NF-*κ*B and MAPK signaling pathways. *J Nat Prod* 2015;**78**:1689-96.

16 Yang D, Yang Z, Chen L, Kuang D, Zou Y, Li J, et al. Dihydromyricetin increases endothelial nitric oxide production and inhibits atherosclerosis through microRNA-21 in apolipoprotein E-deficient mice. *J Cell Mol Med* 2020;**24**:5911-25.

17 Liu TT, Zeng Y, Tang K, Chen X, Zhang W, Xu XL. Dihydromyricetin ameliorates atherosclerosis in LDL receptor deficient mice. *Atherosclerosis* 2017;**262**:39-50.

18 Chen S, Lv K, Sharda A, Deng J, Zeng W, Zhang C, et al. Anti-thrombotic effects mediated by dihydromyricetin involve both platelet inhibition and

endothelial protection. *Pharmacol Res* 2021;**167**:105540.

19 Medina MV, Sapochnik D, Garcia Solá M, Coso O. Regulation of the expression of heme oxygenase-1: signal transduction, gene promoter activation, and beyond. *Antioxid Redox Signal* 2020;**32**:1033-44.

20 Campbell NK, Fitzgerald HK, Dunne A. Regulation of inflammation by the antioxidant haem oxygenase 1. *Nat Rev Immunol* 2021;**21**:411-25.

21 Motterlini R, Otterbein LE. The therapeutic potential of carbon monoxide. *Nat Rev Drug Discov* 2010;**9**:728-43.

22 Jansen T, Daiber A. Direct antioxidant properties of bilirubin and biliverdin. Is there a role for biliverdin reductase?. *Front Pharmacol* 2012;**3**:30.

23 Chen C, Wang Y, Cao Y, Wang Q, Anwaier G, Zhang Q, et al. Mechanisms underlying the inhibitory effects of probucol on elastase-induced abdominal aortic aneurysm in mice. *Br J Pharmacol* 2020;**177**:204-16.

24 Hofmann A, Müglich M, Wolk S, Khorzom Y, Sabarstinski P, Kopaliani I, et al. Induction of heme oxygenase-1 is linked to the severity of disease in human abdominal aortic aneurysm. *J Am Heart Assoc* 2021;**10**:e022747.

25 Ho YC, Wu ML, Gung PY, Chen CH, Kuo CC, Yet SF. Heme oxygenase-1 deficiency exacerbates angiotensin II-induced aortic aneurysm in mice. *Oncotarget* 2016;**7**:67760-76.

26 Qiu R, Chen S, Hua F, Bian S, Chen J, Li G, et al. Betanin prevents experimental abdominal aortic aneurysm progression by modulating the TLR4/NF-κB and Nrf2/HO-1 pathways. *Biol Pharm Bull* 2021;**44**:1254-62.

27 Hamann B, Klimova A, Klotz F, Frank F, Jänichen C, Kapalla M, et al. Regulation of CD163 receptor in patients with abdominal aortic aneurysm and associations with antioxidant enzymes HO-1 and NQO1. *Antioxidants (Basel)* 2023;**12**:947.

28 Wang J, Ye W, Zou J, Yang P, Jin M, Zheng Z, et al. Targeting the smooth muscle cell Keap1–Nrf2–GSDMD–pyroptosis axis by cryptotanshinone prevents abdominal aortic aneurysm formation. *Theranostics* 2024;**14**:6516-42.

29 Imanishi M, Chiba Y, Tomita N, Matsunaga S, Nakagawa T, Ueno M, et al. Hypoxia-inducible factor-1α in smooth muscle cells protects against aortic aneurysms-brief report. *Arterioscler Thromb Vasc Biol* 2016;**36**:2158-62.

30 Takahara Y, Tokunou T, Kojima H, Hirooka Y, Ichiki T. Deletion of hypoxia-inducible factor-1α in myeloid lineage exaggerates angiotensin II-induced

formation of abdominal aortic aneurysm. *Clin Sci (Lond)* 2017;**131**:609-20.

31 Lee JW, Ko J, Ju C, Eltzschig HK. Hypoxia signaling in human diseases and therapeutic targets. *Exp Mol Med* 2019;**51**:1-13.

32 Zou J, Zheng Z, Ye W, Jin M, Yang P, Little PJ, et al. Targeting the smooth muscle cell KEAP1–Nrf2–STING axis with pterostilbene attenuates abdominal aortic aneurysm. *Phytomedicine* 2024;**130**:155696.

33 Xu J, Liu Z, Yang Q, Ma Q, Zhou Y, Cai Y, et al. Adenosine kinase inhibition protects mice from abdominal aortic aneurysm *via* epigenetic modulation of VSMC inflammation. *Cardiovasc Res* 2024;**120**:1202-17.

34 Zeng X, Yang J, Hu O, Huang J, Ran L, Chen M, et al. Dihydromyricetin ameliorates nonalcoholic fatty liver disease by improving mitochondrial respiratory capacity and redox homeostasis through modulation of SIRT3 signaling. *Antioxid Redox Signal* 2019;**30**:163-83.

35 Zeng Y, Peng Y, Tang K, Wang YQ, Zhao ZY, Wei XY, et al. Dihydromyricetin ameliorates foam cell formation *via* LXR*α*–ABCA1/ABCG1-dependent cholesterol efflux in macrophages. *Biomed Pharmacother* 2018;**101**:543-52.

36 Chen Y, Zheng Y, Chen R, Shen J, Zhang S, Gu Y, et al. Dihydromyricetin attenuates diabetic cardiomyopathy by inhibiting oxidative stress, inflammation and necroptosis *via* sirtuin 3 activation. *Antioxidants (Basel)* 2023;**12**:200.

37 Lu H, Sun J, Liang W, Chang Z, Rom O, Zhao Y, et al. Cyclodextrin prevents abdominal aortic aneurysm *via* activation of vascular smooth muscle cell transcription factor EB. *Circulation* 2020;**142**:483-98.

38 Xie D, Wu C, Wang D, Nisma Lena BA, Liu N, Ye G, et al. Wei-fu-chun tablet halted gastric intestinal metaplasia and dysplasia associated with inflammation by regulating the NF-*κ*B pathway. *J Ethnopharmacol* 2024;**318**:117020.

39 Liu Z, Xu J, Ma Q, Zhang X, Yang Q, Wang L, et al. Glycolysis links reciprocal activation of myeloid cells and endothelial cells in the retinal angiogenic niche. *Sci Transl Med* 2020;**12**:eaay1371.

40 Wang J, Liu Z, Lu J, Zou J, Ye W, Li H, et al. SIRT6 regulates endothelium-dependent relaxation by modulating nitric oxide synthase 3 (NOS3). *Biochem Pharmacol* 2023;**209**:115439.

41 Luo S, Kong C, Zhao S, Tang X, Wang Y, Zhou X, et al. Endothelial HDAC1–ZEB2–NuRD complex drives aortic aneurysm and dissection through regulation of protein *s*-sulfhydration. *Circulation* 2023;**147**:1382-403.

42 Dixit M, Zhuang D, Ceacareanu B, Hassid A. Treatment with insulin uncovers the motogenic capacity of nitric oxide in aortic smooth muscle cells: dependence on Gab1 and Gab1–SHP2 association. *Circ Res* 2003;**93**:e113-23.

43 Ma Q, Yang Q, Xu J, Zhang X, Kim D, Liu Z, et al. ATIC-associated *de novo* purine synthesis is critically involved in proliferative arterial disease. *Circulation* 2022;**146**:1444-60.

44 Sun LY, Lyu YY, Zhang HY, Shen Z, Lin GQ, Geng N, et al. Nuclear receptor NR1D1 regulates abdominal aortic aneurysm development by targeting the mitochondrial tricarboxylic acid cycle enzyme aconitase-2. *Circulation* 2022;**146**:1591-609.

45 Yang Q, Xu J, Ma Q, Liu Z, Sudhahar V, Cao Y, et al. PRKAA1/AMPKα1-driven glycolysis in endothelial cells exposed to disturbed flow protects against atherosclerosis. *Nat Commun* 2018;**9**:4667.

46 Yu W, Hu Y, Liu Z, Guo K, Ma D, Peng M, et al. Sorting nexin 3 exacerbates doxorubicin-induced cardiomyopathy *via* regulation of TFRC-dependent ferroptosis. *Acta Pharm Sin B* 2023;**13**:4875-92.

47 Wu Y, Wang J, Zhao T, Chen J, Kang L, Wei Y, et al. Di-(2-ethylhexyl) phthalate exposure leads to ferroptosis *via* the HIF-1α/HO-1 signaling pathway in mouse testes. *J Hazard Mater* 2022;**426**:127807.

48 Guan T, Li M, Song Y, Chen J, Tang J, Zhang C, et al. Phosphorylation of USP29 by CDK1 governs TWIST1 stability and oncogenic functions. *Adv Sci (Weinh)* 2023;**10**:e2205873.

49 Xiao H, Sun X, Lin Z, Yang Y, Zhang M, Xu Z, et al. Gentiopicroside targets PAQR3 to activate the PI3K/AKT signaling pathway and ameliorate disordered glucose and lipid metabolism. *Acta Pharm Sin B* 2022;**12**:2887-904.

50 Ledford BT, Akerman AW, Sun K, Gillis DC, Weiss JM, Vang J, et al. Peptide amphiphile supramolecular nanofibers designed to target abdominal aortic aneurysms. *ACS Nano* 2022;**16**:7309-22.

51 Wilson WR, Anderton M, Schwalbe EC, Jones JL, Furness PN, Bell PR, et al. Matrix metalloproteinase-8 and -9 are increased at the site of abdominal aortic aneurysm rupture. *Circulation* 2006;**113**:438-45.

52 Iida Y, Xu B, Xuan H, Glover KJ, Tanaka H, Hu X, et al. Peptide inhibitor of CXCL4–CCL5 heterodimer formation, MKEY, inhibits experimental aortic aneurysm initiation and progression. *Arterioscler Thromb Vasc Biol*

2013;**33**:718-26.

53 Bossone E, Eagle KA. Epidemiology and management of aortic disease: aortic aneurysms and acute aortic syndromes. *Nat Rev Cardiol* 2021;**18**:331-48.

54 Li X, Yu J, Gong L, Zhang Y, Dong S, Shi J, et al. Heme oxygenase-1(HO-1) regulates Golgi stress and attenuates endotoxin-induced acute lung injury through hypoxia inducible factor-1α (HIF-1α)/HO-1 signaling pathway. *Free Radic Biol Med* 2021;**165**:243-53.

55 Li B, Nasser MI, Masood M, Adlat S, Huang Y, Yang B, et al. Efficiency of traditional Chinese medicine targeting the Nrf2/HO-1 signaling pathway. *Biomed Pharmacother* 2020;**126**:110074.

56 Stegen S, Laperre K, Eelen G, Rinaldi G, Fraisl P, Torrekens S, et al. HIF-1α metabolically controls collagen synthesis and modification in chondrocytes. *Nature* 2019;**565**:511-5.

57 Lifshits LA, Rabin M, Tohar R, Netti F, Gabay M, Sova M, et al. Enhancement of collagen-I levels in human gingival fibroblasts by small molecule activation of HIF-1α. *J Agric Food Chem* 2023;**71**:7829-35.

58 Semenza GL. Hypoxia-inducible factor 1 and cardiovascular disease. *Annu Rev Physiol* 2014;**76**:39-56.

59 Wu J, Li S, Li C, Cui L, Ma J, Hui Y. The non-canonical effects of heme oxygenase-1, a classical fighter against oxidative stress. *Redox Biol* 2021;**47**:102170.

60 Liu CL, Liu X, Zhang Y, Liu J, Yang C, Luo S, et al. Eosinophils protect mice from angiotensin-II perfusion-induced abdominal aortic aneurysm. *Circ Res* 2021;**128**:188-202.

61 Batra R, Suh MK, Carson JS, Dale MA, Meisinger TM, Fitzgerald M, et al. IL-1β (interleukin-1β) and TNF-α (tumor necrosis factor-α) impact abdominal aortic aneurysm formation by differential effects on macrophage polarization. *Arterioscler Thromb Vasc Biol* 2018;**38**:457-63.

62 Xiong W, MacTaggart J, Knispel R, Worth J, Persidsky Y, Baxter BT. Blocking TNF-α attenuates aneurysm formation in a murine model. *J Immunol* 2009;**183**:2741-6.

63 Yu M, Dong A, Chen C, Xu S, Cao Y, Liu S, et al. Thermosensitive hydrogel containing doxycycline exerts inhibitory effects on abdominal aortic aneurysm induced by pancreatic elastase in mice. *Adv Healthc Mater* 2017;**6**. Available

from: https://doi.org/10.1002/adhm.201700671.

64 Gao M, Qi Z, Deng M, Huang H, Xu Z, Guo G, et al. The deubiquitinase USP7 regulates oxidative stress through stabilization of HO-1. *Oncogene* 2022;**41**:4018-27.

65 Baxter BT, Matsumura J, Curci JA, McBride R, Larson L, Blackwelder W, et al. Effect of doxycycline on aneurysm growth among patients with small infrarenal abdominal aortic aneurysms: a randomized clinical trial. *JAMA* 2020;**323**:2029-38.

66 Bicknell CD, Kiru G, Falaschetti E, Powell JT, Poulter NR. An evaluation of the effect of an angiotensin-converting enzyme inhibitor on the growth rate of small abdominal aortic aneurysms: a randomized placebo-controlled trial (AARDVARK). *Eur Heart J* 2016;**37**:3213-21.

67 Lederle FA, Noorbaloochi S, Nugent S, Taylor BC, Grill JP, Kohler TR, et al. Multicentre study of abdominal aortic aneurysm measurement and enlargement. *Br J Surg* 2015;**102**:1480-7.

68 Zhou T, Wang Q, Phan N, Ren J, Yang H, Feldman CC, et al. Identification of a novel class of RIP1/RIP3 dual inhibitors that impede cell death and inflammation in mouse abdominal aortic aneurysm models. *Cell Death Dis* 2019;**10**:226.

69 Yan H, Cui B, Zhang X, Fu X, Yan J, Wang X, et al. Antagonism of Toll-like receptor 2 attenuates the formation and progression of abdominal aortic aneurysm. *Acta Pharm Sin B* 2015;**5**:176-87.

70 Lei C, Kan H, Xian X, Chen W, Xiang W, Song X, et al. FAM3A reshapes VSMC fate specification in abdominal aortic aneurysm by regulating KLF4 ubiquitination. *Nat Commun* 2023;**14**:5360.

71 Jiang WC, Chen CM, Hamdin CD, Orekhov AN, Sobenin IA, Layne MD, et al. Therapeutic potential of heme oxygenase-1 in aneurysmal diseases. *Antioxidants (Basel)* 2020;**9**:1150.

72 Hou X, Yang S, Zheng Y. Licochalcone a attenuates abdominal aortic aneurysm induced by angiotensin II *via* regulating the miR-181b/SIRT1/HO-1 signaling. *J Cell Physiol* 2019;**234**:7560-8.

73 Chan WL, Pejnovic N, Hamilton H, Liew TV, Popadic D, Poggi A, et al. Atherosclerotic abdominal aortic aneurysm and the interaction between

autologous human plaque-derived vascular smooth muscle cells, type 1 NKT, and helper T cells. *Circ Res* 2005;**96**:675-83.

74 Nakahashi TK, Hoshina K, Tsao PS, Sho E, Sho M, Karwowski JK, et al. Flow loading induces macrophage antioxidative gene expression in experimental aneurysms. *Arterioscler Thromb Vasc Biol* 2002;**22**:2017-22.

75 Azuma J, Wong RJ, Morisawa T, Hsu M, Maegdefessel L, Zhao H, et al. Heme oxygenase-1 expression affects murine abdominal aortic aneurysm progression. *PLoS One* 2016;**11**:e0149288.

76 Kopacz A, Werner E, Grochot-Przęczek A, Klóska D, Hajduk K, Neumayer C, et al. Simvastatin attenuates abdominal aortic aneurysm formation favoured by lack of Nrf2 transcriptional activity. *Oxid Med Cell Longev* 2020;**2020**:6340190.

77 Ye W, Wang J, Little PJ, Zou J, Zheng Z, Lu J, et al. Anti-atherosclerotic effects and molecular targets of ginkgolide B from *Ginkgo biloba*. *Acta Pharm Sin B* 2024;**14**:1-19.

78 Zou J, Wang J, Ye W, Lu J, Li C, Zhang D, et al. *Citri reticulatae pericarpium* (Chenpi): a multi-efficacy pericarp in treating cardiovascular diseases. *Biomed Pharmacother* 2022;**154**:113626.

79 Alam J, Cook JL. How many transcription factors does it take to turn on the heme oxygenase-1 gene?. *Am J Respir Cell Mol Biol* 2007;**36**:166-74.

80 Song J, Zhang X, Liao Z, Liang H, Chu L, Dong W, et al. 14-3-3ζ inhibits heme oxygenase-1 (HO-1) degradation and promotes hepatocellular carcinoma proliferation: involvement of STAT3 signaling. *J Exp Clin Cancer Res* 2019;**38**:3.

81 Gu X, Nardone C, Kamitaki N, Mao A, Elledge SJ, Greenberg ME. The midnolin–proteasome pathway catches proteins for ubiquitination-independent degradation. *Science* 2023;**381**:eadh5021.

82 Jia Y, Zhang L, Liu Z, Mao C, Ma Z, Li W, et al. Targeting macrophage TFEB-14-3-3 epsilon interface by naringenin inhibits abdominal aortic aneurysm. *Cell Discov* 2022;**8**:21.

83 Wang L, Wang B, Li H, Lu H, Qiu F, Xiong L, et al. Quercetin, a flavonoid with anti-inflammatory activity, suppresses the development of abdominal aortic aneurysms in mice. *Eur J Pharmacol* 2012;**690**:133-41.

84 Ran L, Wang X, Lang H, Xu J, Wang J, Liu H, et al. *Ampelopsis grossedentata* supplementation effectively ameliorates the glycemic control in patients with

type 2 diabetes mellitus. *Eur J Clin Nutr* 2019;**73**:776-82.

85 Liu D, Mao Y, Ding L, Zeng XA. Dihydromyricetin: a review on identification and quantification methods, biological activities, chemical stability, metabolism and approaches to enhance its bioavailability. *Trends Food Sci Technol* 2019;**91**:586-97.

86 Ruan LP, Yu BY, Fu GM, Zhu DN. Improving the solubility of ampelopsin by solid dispersions and inclusion complexes. *J Pharm Biomed Anal* 2005;**38**:457-64.

87 Dalcin AJF, Vizzotto BS, Bochi GV, Guarda NS, Nascimento K, Sagrillo MR, et al. Nanoencapsulation of the flavonoid dihydromyricetin protects against the genotoxicity and cytotoxicity induced by cationic nanocapsules. *Colloids Surf B* 2019;**173**:798-805.

Figure captions

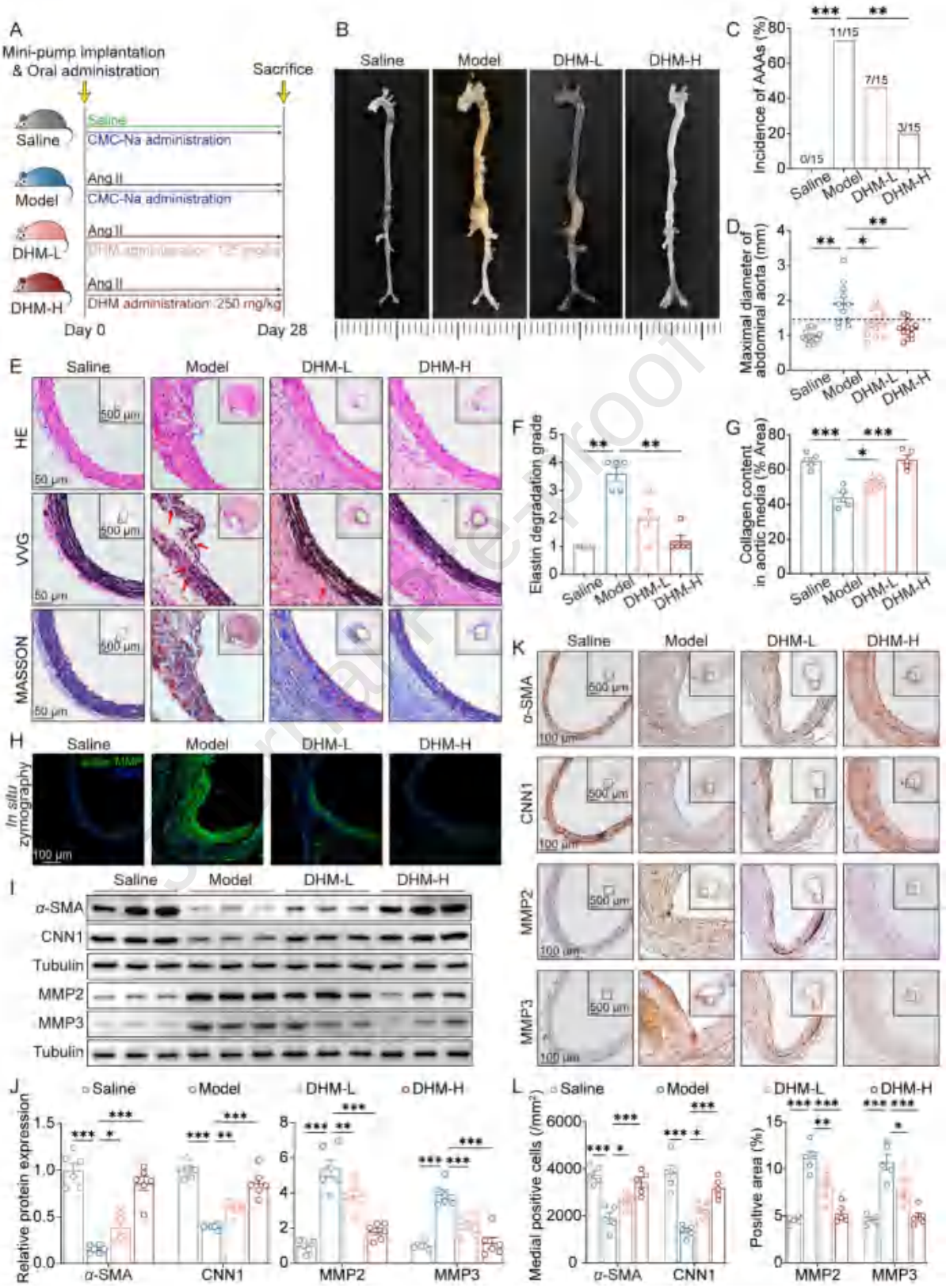

Figure 1 DHM prevents AAA formation and maintains vascular morphology in the Ang II-induced murine AAA model. (A–L) In the murine AAA model, 12-week-old male

ApoE$^{-/-}$ mice were infused with either saline or Ang II (1000 ng/kg/min) for a period of four weeks. On the day the AAA was induced, 0.5% CMC-Na, low-dose DHM (DHM-L, 125 mg/kg), or high-dose DHM (DHM-H, 250 mg/kg) were administered (*p.o.*), respectively, once per day. (A) Induction of AAA and administration regimens. (B) Representative images of abdominal aortic aneurysm. (C) AAA incidence. (D) Maximal diameter of the abdominal aorta was assessed in four groups (n = 11–15). (E) Representative images of vessel sections stained with hematoxylin and eosin (H&E), Verhoeff-Van Gieson (VVG), and Masson's trichrome staining. In VVG staining, the dark color represents elastin, and red triangles indicate that elastin is broken. In Masson's trichrome staining, the blue color represents collagen deposition. (F) The grade of elastin degradation was evaluated (n = 5). (G) Collagen in the aortic media was quantitatively analyzed by Masson's trichrome staining (n = 5). (H) *In situ* zymography immunofluorescence images for assessing MMP activities. (I, J) Representative Western blot and quantitative analysis of α-SMA, CNN1, MMP2, and MMP3 protein levels in murine aorta (n = 6). (K, L) Representative images and quantitative analysis of immunohistochemical staining for α-SMA, CNN1, MMP2, and MMP3 (n = 5). Data are presented as mean ± SEM; $^{*}P < 0.05$, $^{**}P < 0.01$, $^{***}P < 0.001$. Fisher's exact test for (C), Brown–Forsythe and Welch ANOVA test with Dunnett's T3 multiple comparison for (D), non-parametric Kruskal–Wallis test followed by Dunn's *post hoc* analysis for (F), and one-way ANOVA followed by a Bonferroni' *post hoc* analysis for (G), (J) and (L).

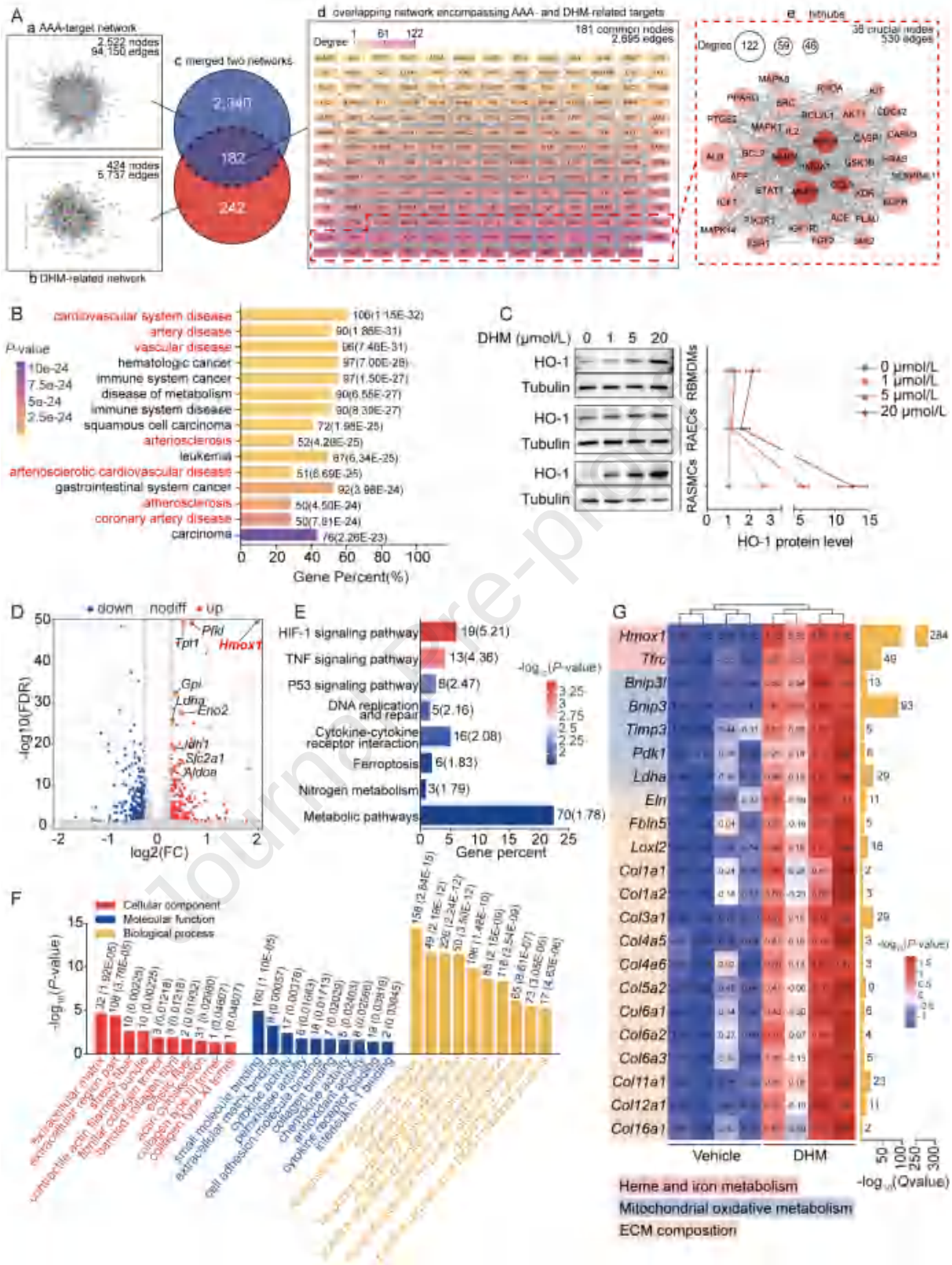

Figure 2 DHM promotes the activation of the SMC HIF-1α/HO-1 pathway based on network pharmacology prediction and RNA-seq analyses. (A, B) 2522 AAA-associated targets and 424 DHM-related targets were collected from publicly available databases.

Merging these networks revealed 182 common genes, potential targets for DHM in AAA prevention. Cytoscape analysis provided degree values for each target; those exceeding 1.5 times of the mean were considered key targets in restraining AAA for DHM. Additionally, the 182 common targets were subjected to DO, KEGG, and GO analyses. (A) The process of screening potential and core targets of DHM in its action on AAA. (B) The DO enrichment analysis revealed that the 182 common genes were primarily associated with vascular diseases. In this analysis, the color and length of the bands were utilized to signify the *P*-value and the percentage of genes. (C) The expression levels of HO-1 protein were quantified in RBMDMs, RAECs, and RASMCs following a 24-h treatment with varying concentrations of DHM (0, 1, 5, and 20 μmol/L) (n = 5). (D–G) For RNA-seq analysis, 20 μmol/L DHM or an equal volume of DMSO were treated with RASMCs for a duration of 3 h. Subsequently, both groups were exposed to TNF-α for an additional 3 h, and cell RNA was collected. (D) Comparing TNF-α stimulation to co-treatment with DHM and TNF-α, the volcano plot indicated the magnitude and significance of the changes in gene expression in RASMCs. (E, F) The KEGG and GO enrichment analyses revealed how DHM influences RASMCs at the molecular and cellular levels. (G) The heatmap showed DHM-upregulated genes related to heme and iron metabolism, mitochondrial oxidative metabolism, and ECM composition in the RNA-seq analysis. All DO, KEGG, and GO analyses were performed using the OmicShare tools, a free online platform for data analysis (https://www.omicshare.com/tools). Two-way ANOVA followed by Bonferroni's *post hoc* testing for (C).

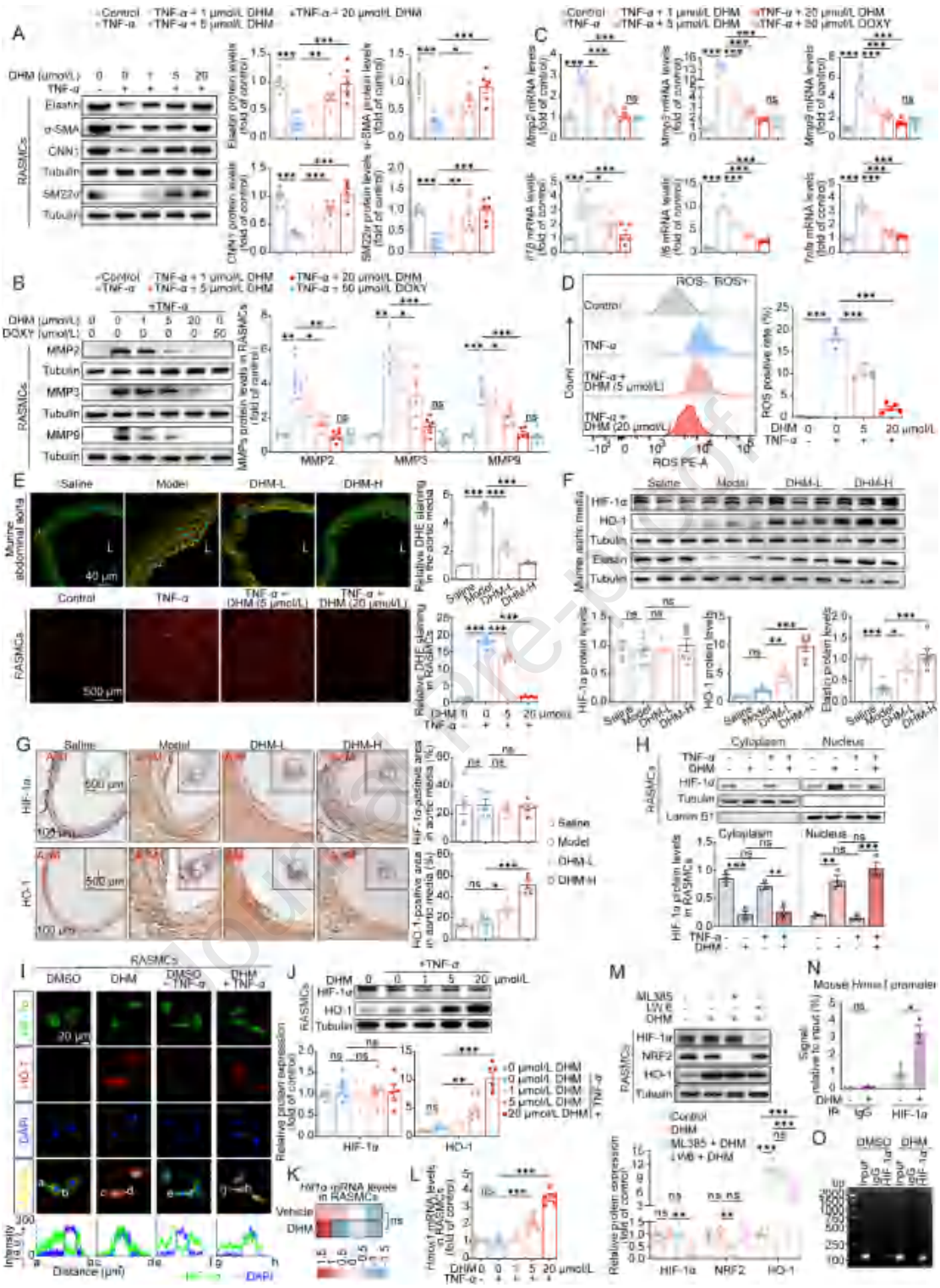

Figure 3 DHM enhances HO-1 protein transcription by facilitating HIF-1*α* nuclear translocation, leading to anti-inflammatory and antioxidant effects, preserving ECM homeostasis, and inhibiting SMC phenotypic changes. (A, B) Western blot analysis of the protein levels of elastin, *α*-SMA, SM22*α*, CNN1, MMP2, MMP3, and MMP9 (*n* = 6). (C) RT-qPCR analysis of *Mmp2*, *Mmp3*, *Mmp9*, *Il1β*, *Il6*, and *Tnfα* expression in

different groups of RASMCs (n = 5). (D) Intracellular levels of ROS were detected by flow cytometry (n = 5). (E) Representative images and quantitative analysis of DHE staining in murine abdominal aorta (n = 3) and RASMCs (n =5) (L: lumen). (F) Representative Western blot and quantitative analysis of HIF-1α, HO-1, and elastin protein levels in murine aortas which adventitial tissue was removed (n = 6). (G) Representative images and quantitative analysis of immunohistochemical staining for HIF-1α and HO-1 (n =5) (M: media; A: adventitia). (H) Western blot analysis and quantitative assessment of HIF-1α in the cytoplasm and nuclei of RASMCs (n = 3). (I) Immunofluorescence images of representative samples displayed enhanced nuclear translocation of HIF-1α and HO-1 expression following DHM treatment. ImageJ software measured the line profiles of the mean fluorescence intensity of HIF-1α and DAPI signals. (J) Western blot analysis and quantitative data indicated that DHM treatment specifically upregulated the expression of HO-1 protein while leaving the expression of HIF-1α unaffected (n = 6). (K) According to RNA-seq results, the heatmap revealed changes in *Hif1α* expression after DHM treatment (n = 4). (L) RT-qPCR analysis of *Hmox1* expression at different DHM concentrations in RASMCs (n = 5). (M) Western blot analysis showed that LW 6 partially reversed DHM-induced HO-1 protein expression, although levels remained significantly higher than the control group (n = 5). (N, O) ChIP-qPCR experiment was conducted on MASMCs after exposure to either DMSO or DHM. Antibodies specific to HIF-1α were used to target and amplify the promoter region of *Hmox1* using qPCR (n = 3). Data are presented as mean ± SEM; *$P < 0.05$, **$P < 0.01$, ***$P < 0.001$, and ns means no significance. One-way ANOVA followed by a Bonferroni' *post hoc* analysis for (A), (C–H), (J), (L), and (M). One-way ANOVA followed by a Bonferroni' *post hoc* analysis or Brown-Forsythe and Welch ANOVA test with Dunnett's T3 multiple comparison for (B). Two-way ANOVA followed by Bonferroni' test (N) and unpaired t test (K).

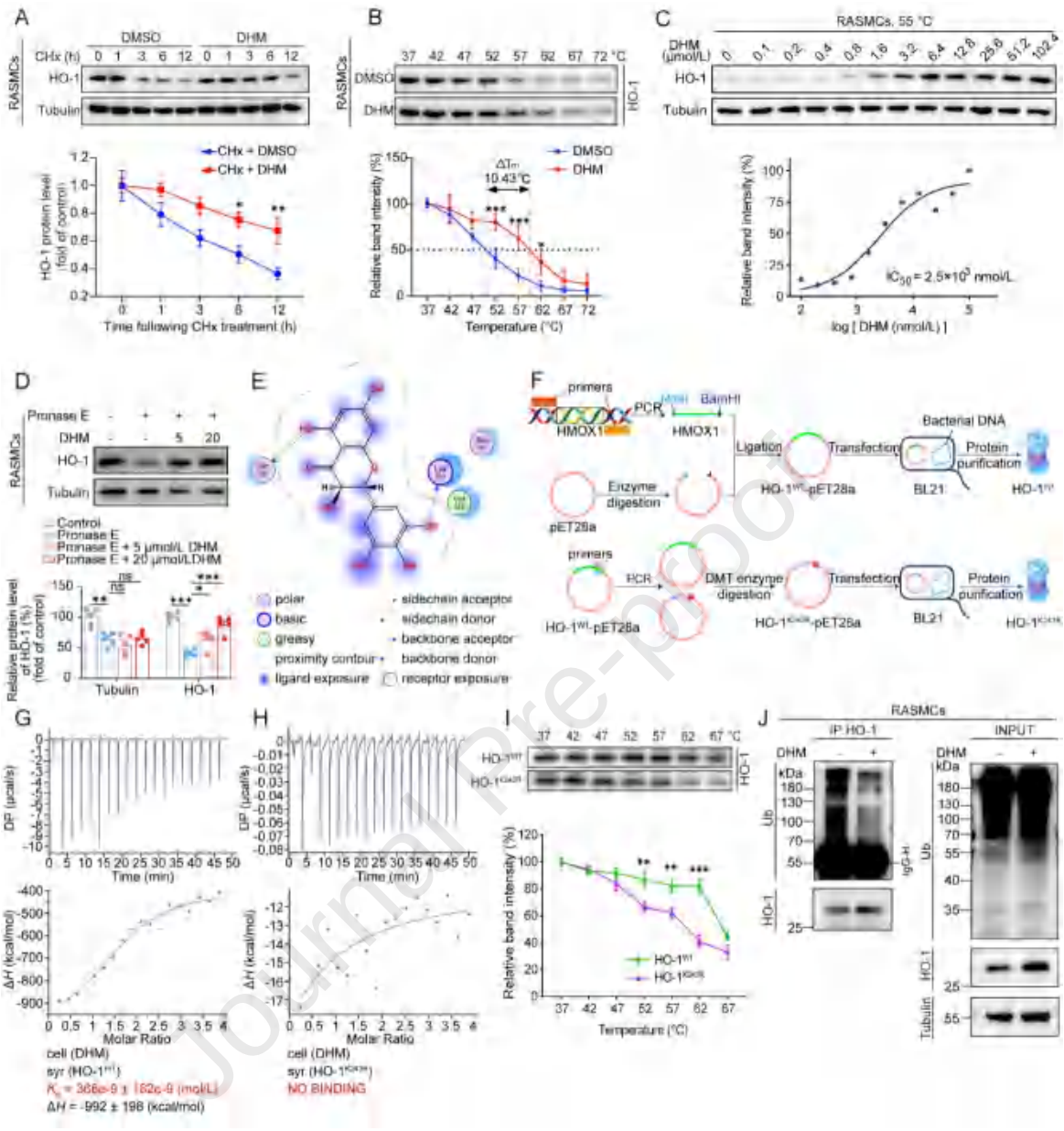

Figure 4 DHM impedes HO-1 degradation by binding to Lys243 of HO-1 protein. (A) Following a 1-h pre-treatment with 20 μmol/L DHM, RASMCs were subjected to varying times of exposure to 50 μmol/L CHx. Western blot comparison between DMSO and DHM treatment of HO-1 protein levels after protein synthesis inhibition (n =5). (B, C) CETSA tests on HO-1 with and without DHM were done at different temperatures and dosages. RASMCs were treated with 20 μmol/L DHM or DMSO for 4 h, resulting in eight aliquots of cell lysates. Each aliquot was heated at 37–72 °C for 5 min. After that, they chilled for 3 min at room temperature. Two liquid nitrogen freeze-thaw cycles were performed on these samples. These samples underwent Western blot analysis after

centrifugation. The ITDRF-CETSA experiment included exposing cells to different DHM doses (0–102.4 μmol/L) over 4 h. These cells' protein lysates were cooked at 55 °C for 5 min. Western blot studies were performed when these protein lysates were properly lysed. (D) The cell lysis was treated with DHM at concentrations of 0, 5, and 20 μmol/L, and then underwent Pronase E digestion. The protein concentration of HO-1 was assessed by Western blot analysis and quantified using Image J software. (E) The 2D image illustrated DHM's interaction with specific amino acids, Lys243 and Gln245. Hydrogen bonds are denoted by green and blue dotted lines. (F) A flowchart showed the construction of HO-1^{WT} and HO-1^{K243R} plasmids and the subsequent protein purification process. (G, H) Isothermal titration plot of 2 μmol/L DHM (in cells) with 40 μmol/L HO-1^{WT} or HO-1^{K243R} (in syringes). The inset provided a graphical representation of the thermodynamic parameters, including K_D and ΔH. The solid line represents the optimal nonlinear least-squares fit to a single binding site model. (I) Western blot analysis was used to assess the impact of DMSO and DHM treatment on HO-1^{WT} and HO-1^{K243R} at different temperatures ($n = 3$). (J) Co-IP of HO-1 in RASMCs treated with DMSO/DHM was performed to confirm the interaction between HO-1 and ubiquitin. Data are presented as mean ± SEM; $^{*}P < 0.05$, $^{**}P < 0.01$, $^{***}P < 0.001$, and ns means no significance. Two-way ANOVA followed by Bonferroni' test for (A–C), and (I). One-way ANOVA followed by a Bonferroni' *post hoc* analysis for (D).

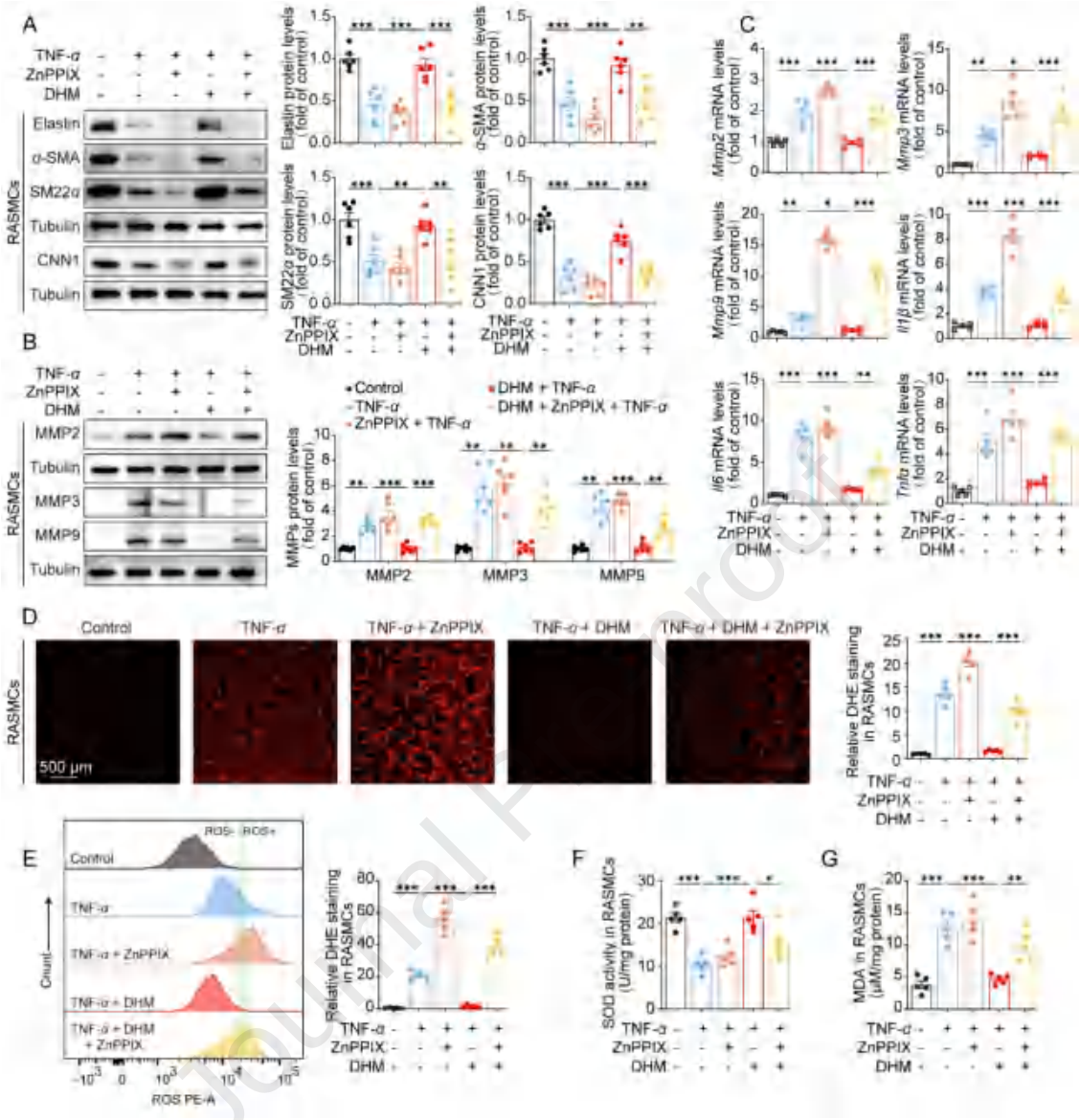

Figure 5 Competitive HO-1 inhibitor reverses DHM's regulation of ECM composition, cellular phenotypic transition, and anti-inflammatory and antioxidative effects in RASMCs. (A–G) RASMCs were pre-treated with ZnPPIX for 1 h and then added 20 μmol/L DHM for 3 h. After being treated with 10 ng/mL TNF-*α*, cells were collected for RT-qPCR experiments at 9 h and for Western blot at 24 h. For ROS detection, cells were incubated in DHE for 1 h before flow cytometry or photography. To detect SOD activity and MDA contents, RASMCs were exposed to TNF-*α* for 12 h upon pre-treating ZnPPIX and DHM. (A, B) Western blot analysis of the protein levels of elastin, *α*-SMA, SM22*α*, CNN1, MMP2, MMP3, and MMP9 (*n* = 6). (C) RT-qPCR analysis of *Mmp2*, *Mmp3*, *Mmp9*, *Il1β*, *Il6*, and *Tnfα* expression in different groups of RASMCs (*n*

= 5). (D) Representative images and quantitative analysis of DHE staining in RASMCs (*n* =5). (E) Intracellular levels of ROS were detected by flow cytometry (*n* = 5). (F–G) Change of SOD and MDA levels after ZnPPIX and DHM treatment (*n* =5). Data are presented as mean ± SEM; **P* < 0.05, ***P* < 0.01, ****P* < 0.001, and ns means no significance. One-way ANOVA followed by Bonferroni' test for (A–G).

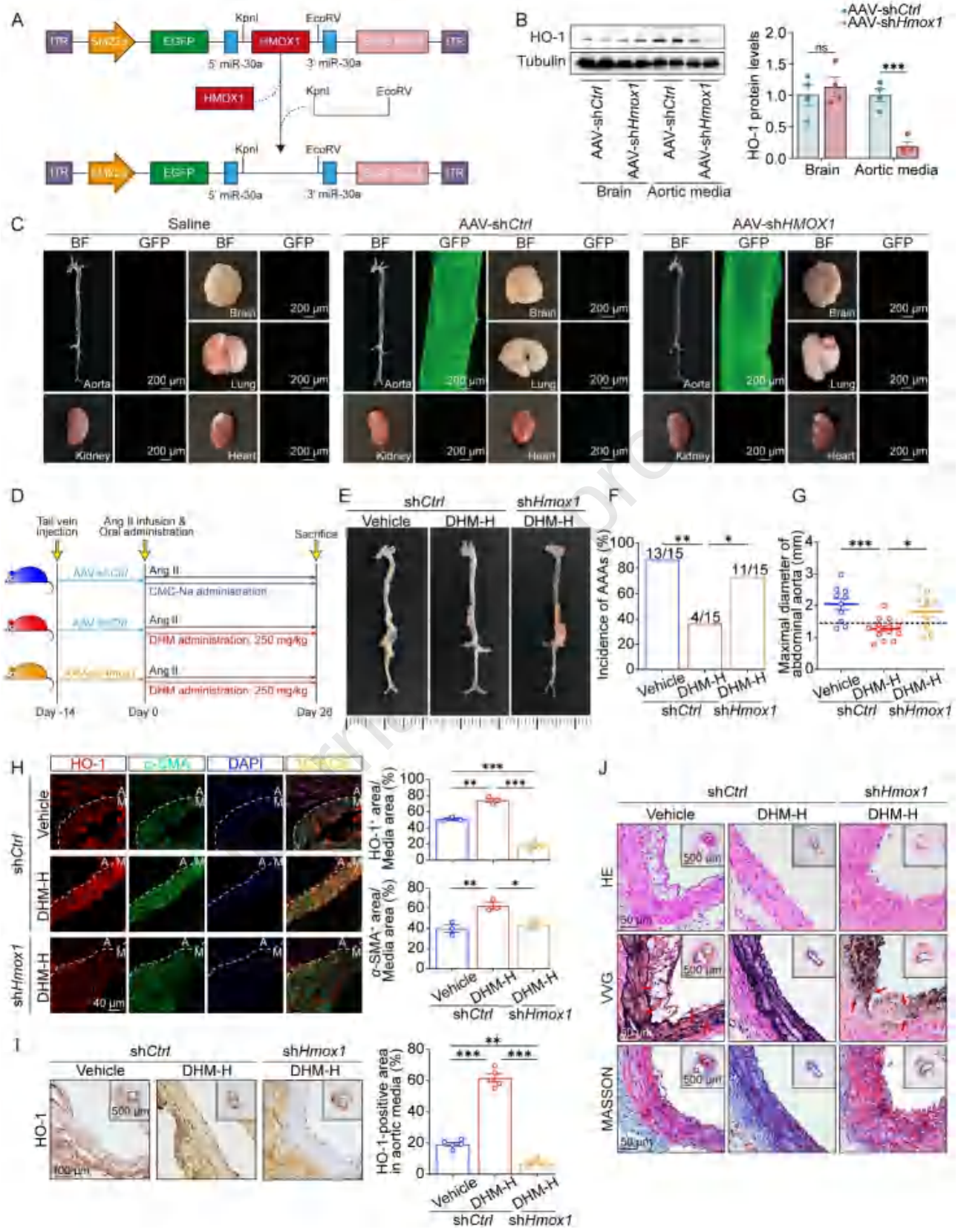

Figure 6 SMC-specific *Hmox1* knockdown abolishes the anti-AAA effect of DHM in Ang II-induced murine AAA model. (A, B) Construction and verification of SMC-specific *Hmox1* knockdown mice. (C) Mouse organs were collected for

GFP-fluorescence detection. Both bright-field and fluorescence images were captured under the same conditions. (D) Induction of AAA and administration regimens. (E) Representative images of abdominal aortic aneurysm. (F) AAA incidence. (G) Maximal diameter of the abdominal aorta (n = 10–14). (H) Images and quantitative analysis of HO-1 and α-SMA immunofluorescence in the murine abdominal aorta (n = 3) (M: media; A: adventitia). (I) Representative images and quantitative analysis of immunohistochemical staining for HO-1 (n =5). (J) Representative images of vessel sections stained with H&E, VVG, and Masson's trichrome staining. Data are presented as mean ± SEM; *P < 0.05, **P < 0.01, ***P < 0.001, and ns means no significance. Fisher's exact test for (F), unpaired t test for (B), and one-way ANOVA followed by Bonferroni' test for (G), (H), and (I).

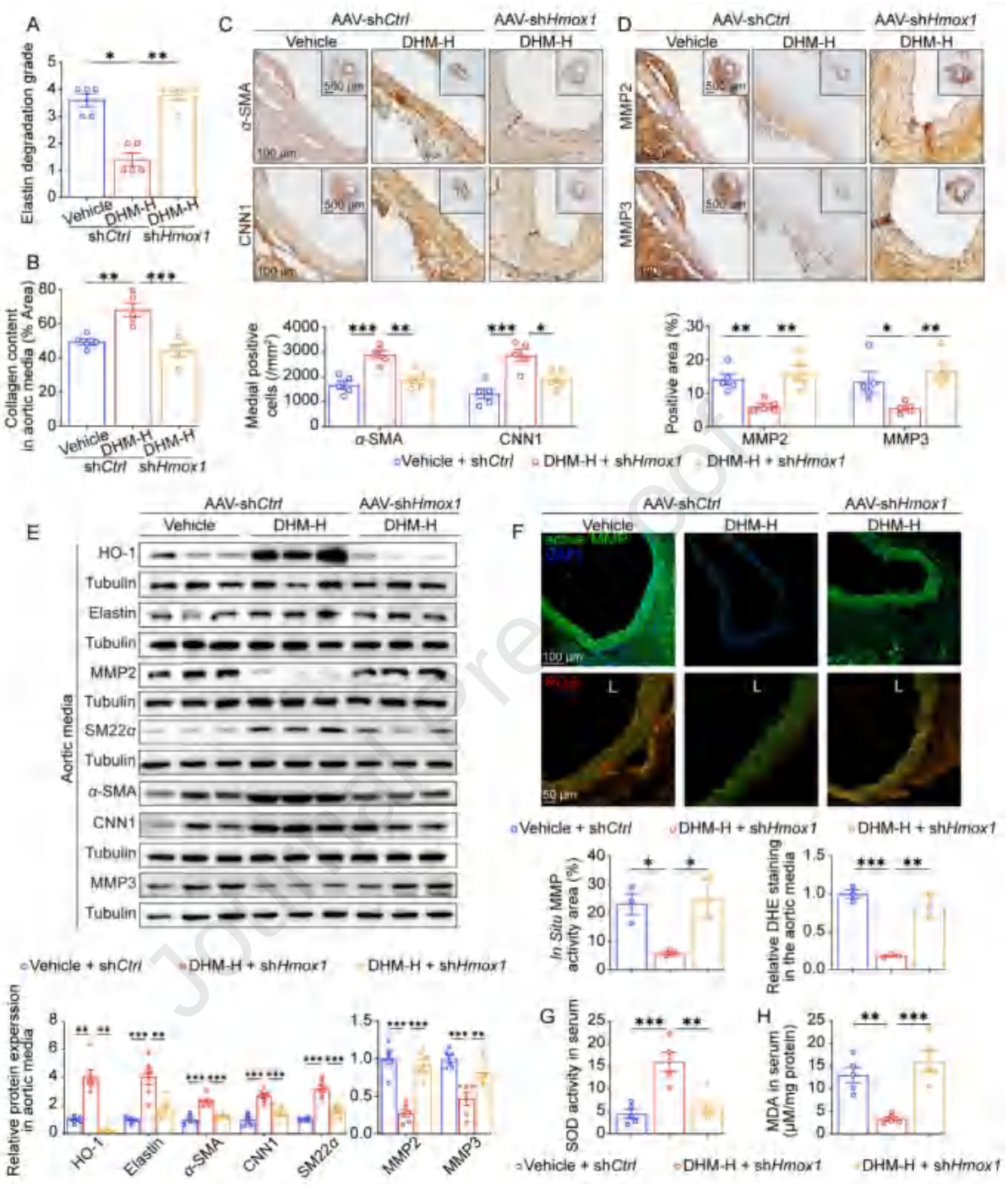

Figure 7 SMC-specific *Hmox1* knockdown abolishes the effect of DHM on anti-inflammatory, antioxidant, and inhibiting MMP activity and generation *in vivo*. (A) The grade of elastin degradation was evaluated (n = 5). (B) Collagen in the aortic media was quantitatively analyzed by Masson's trichrome staining (n = 5). (C, D) Representative images and quantitative analysis of immunohistochemical staining for α-SMA, CNN1, MMP2, and MMP3 (n = 5). (E) Representative Western blot and quantitative analysis of HO-1, elastin, α-SMA, CNN1, SM22α, MMP2, and MMP3 protein levels in murine

aortas which adventitial tissue was removed (n = 6). (F) MMP activities were assessed using *in situ* zymography immunofluorescence pictures, while ROS levels were determined using DHE immunofluorescence images (n = 3). (G, H) Alteration of SOD and MDA concentrations in different groups (n = 5). Data are presented as mean ± SEM; *P < 0.05, **P < 0.01, ***P < 0.001. Non-parametric Kruskal–Wallis test followed by Dunn's *post hoc* analysis for (A), one-way ANOVA followed by Bonferroni' test for (B), (C), (D), (P), (F), (G), and (H). One-way ANOVA followed by a Bonferroni' *post hoc* analysis or Brown–Forsythe and Welch ANOVA test with Dunnett's T3 multiple comparison for (E).

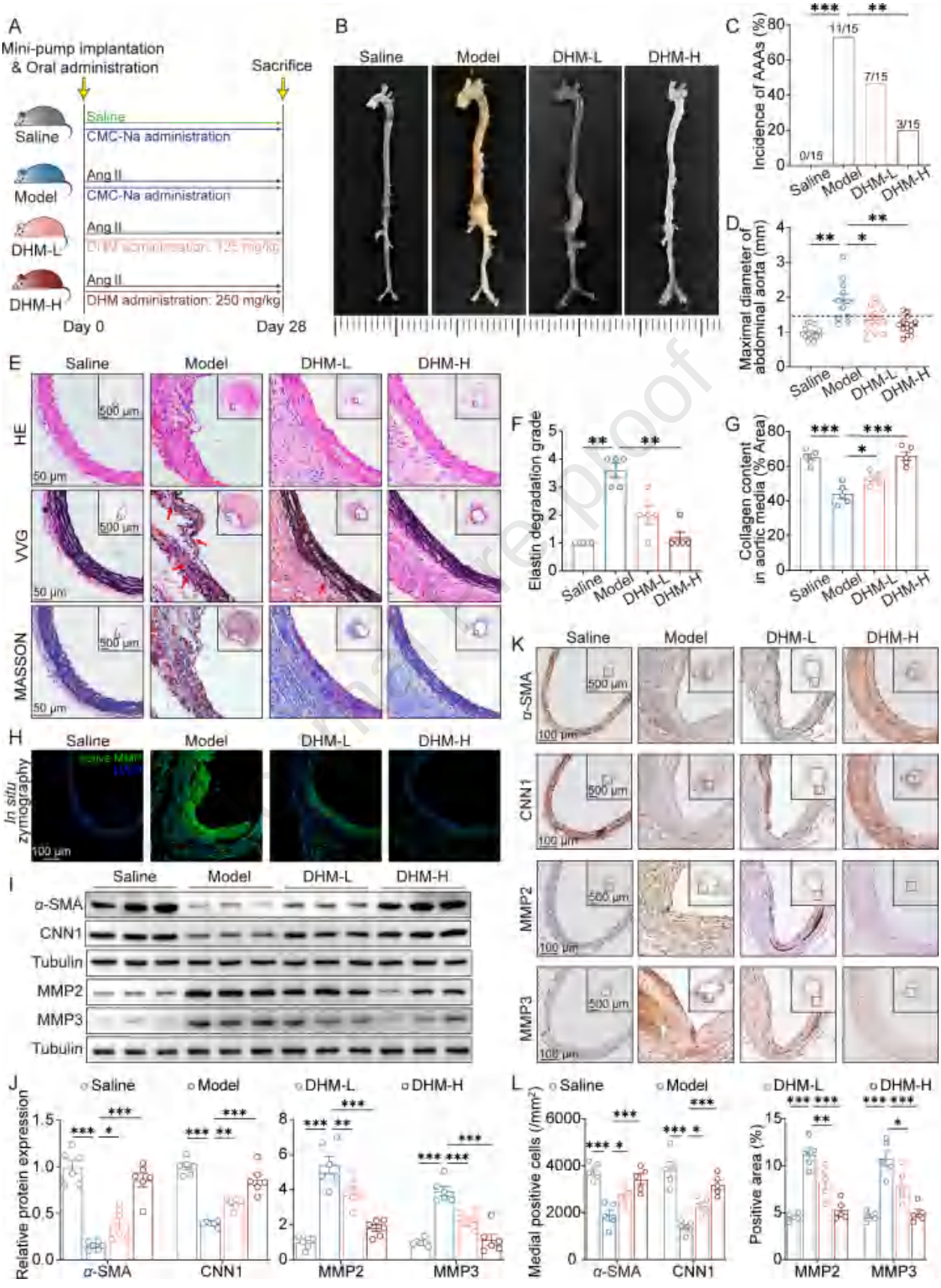
A
Mini-pump implantation
& Oral administration
Sacrifice
Saline
Saline
CMC-Na administration
Model
Ang II
CMC-Na administration
DHM-L
Ang II
DHM-H
Ang II
DHM administration: 250 mg/kg
Day 0
Day 28
B
Saline
Model
DHM-L
DHM-H
C
Incidence of AAAs (%)
0/15
11/15
7/15
3/15
D
Maximal diameter of abdominal aorta (mm)
E
HE
VVG
MASSON
500 μm
50 μm
F
Elastin degradation grade
G
Collagen content in aortic media (% Area)
H
In situ zymography
Active MMP
DAPI
100 μm
I
α-SMA
CNN1
Tubulin
MMP2
MMP3
Tubulin
K
α-SMA
CNN1
MMP2
MMP3
100 μm
J
Relative protein expression
α-SMA
CNN1
MMP2
MMP3
L
Medial positive cells (/mm²)
Positive area (%)

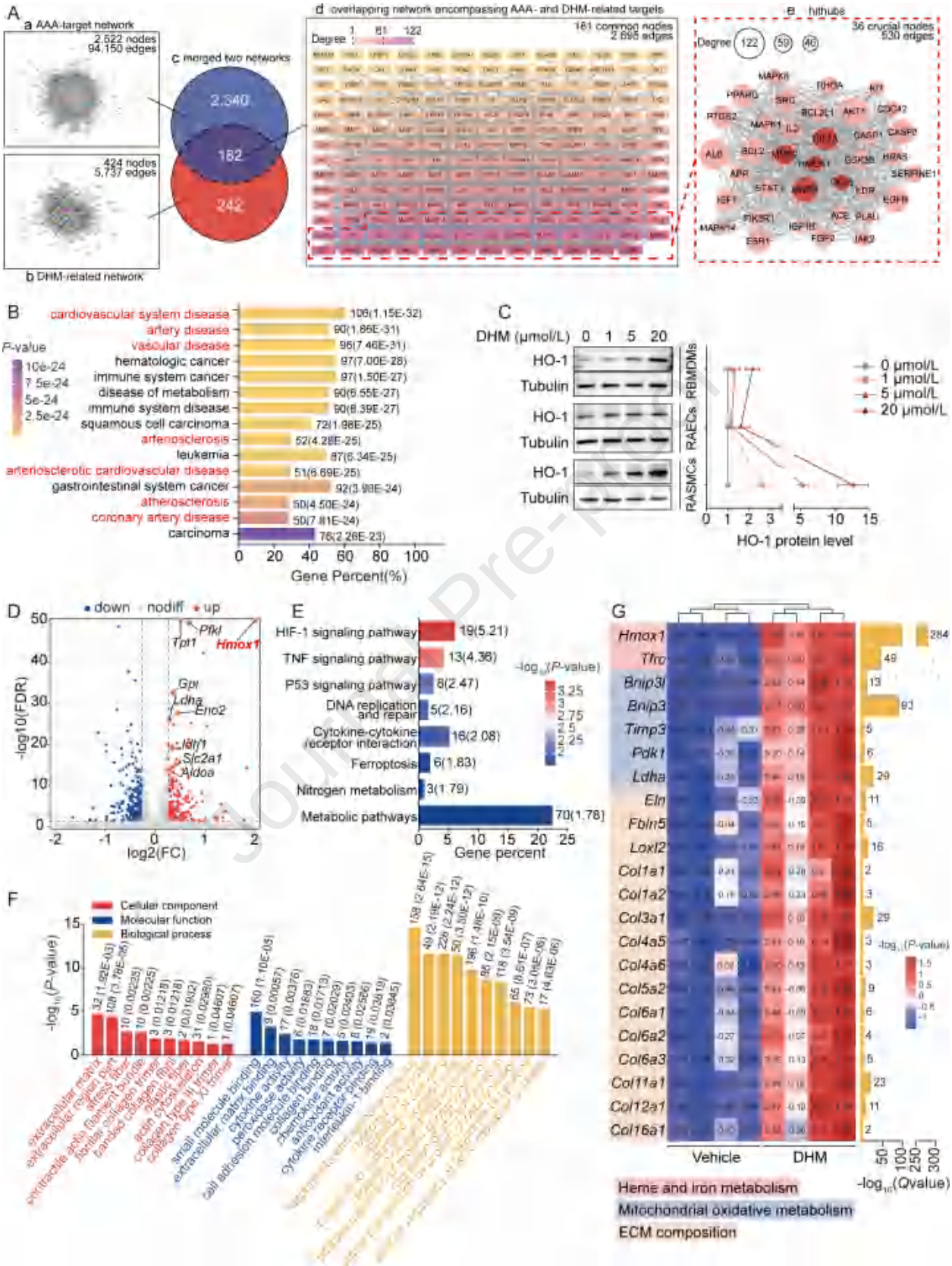

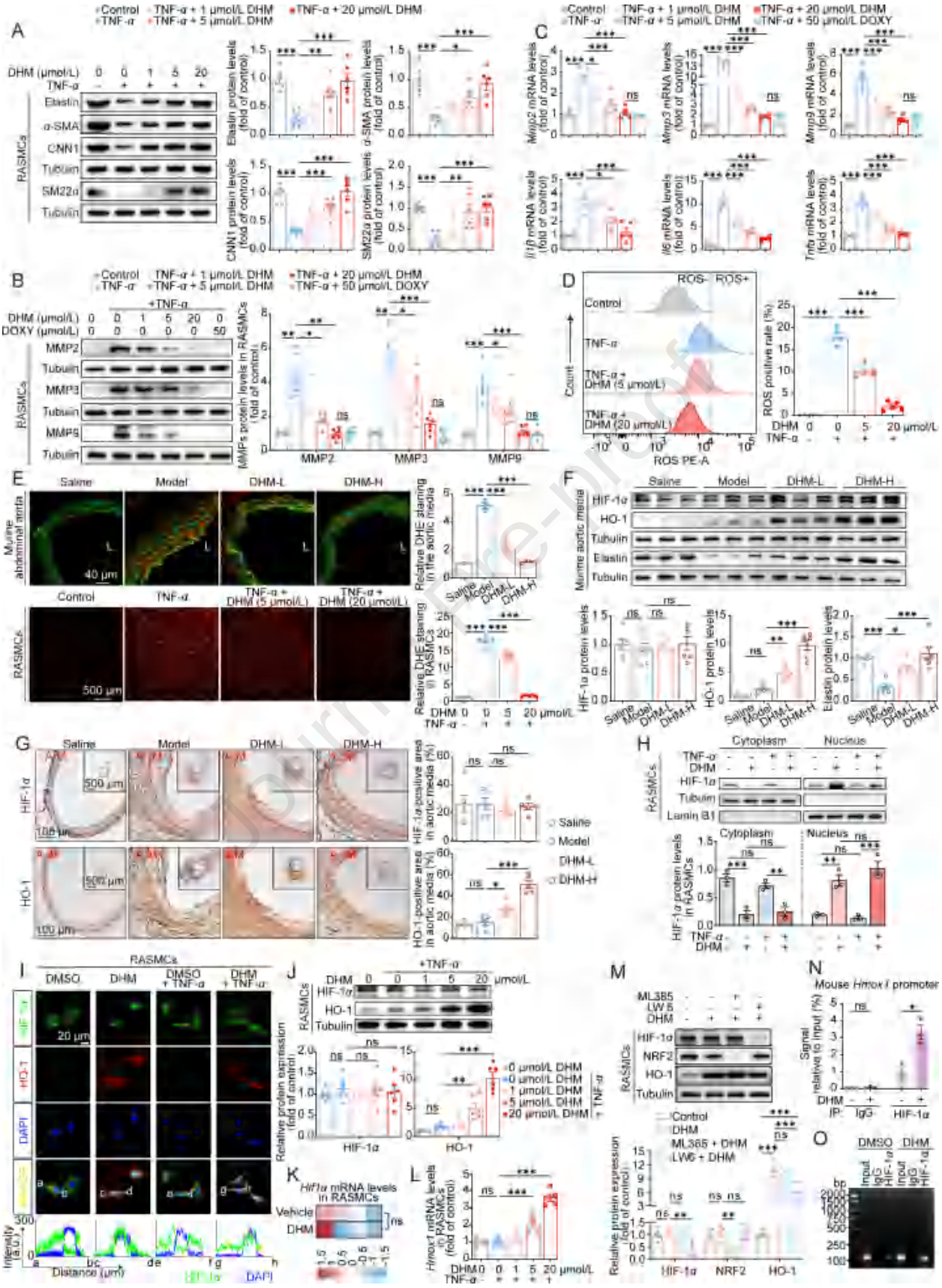
A
Control
TNF-α
TNF-α + 1 μmol/L DHM
TNF-α + 5 μmol/L DHM
TNF-α + 20 μmol/L DHM
DHM (μmol/L) 0 0 1 5 20
TNF-α - + + + +
RASMCs
Elastin
α-SMA
CNN1
Tubulin
SM22α
Tubulin
Elastin protein levels (fold of control)
α-SMA protein levels (fold of control)
CNN1 protein levels (fold of control)
SM22α protein levels (fold of control)
B
TNF-α + 50 μmol/L DOXY
DOXY (μmol/L) 0 0 0 0 0 50
MMP2
MMP3
MMP9
MMP's protein levels in RASMCs (fold of control)
C
Mmp2 mRNA levels (fold of control)
Mmp3 mRNA levels (fold of control)
Mmp9 mRNA levels (fold of control)
Il1β mRNA levels (fold of control)
Il6 mRNA levels (fold of control)
Tnfα mRNA levels (fold of control)
D
ROS-
ROS+
Control
TNF-α
TNF-α + DHM (5 μmol/L)
TNF-α + DHM (20 μmol/L)
Count
ROS PE-A
ROS positive rate (%)
E
Saline
Model
DHM-L
DHM-H
Murine abdominal aorta
Murine aortic media
40 μm
Control
TNF-α
TNF-α + DHM (5 μmol/L)
TNF-α + DHM (20 μmol/L)
RASMCs
500 μm
Relative DHE staining in the aortic media
Relative DHE staining in RASMCs
F
HIF-1α
HO-1
Tubulin
Elastin
HIF-1α protein levels
HO-1 protein levels
Elastin protein levels
G
HIF-1α
HO-1
500 μm
100 μm
HIF-1α-positive area in aortic media (%)
HO-1-positive area in aortic media (%)
H
Cytoplasm
Nucleus
RASMCs
TNF-α
DHM
HIF-1α
Tubulin
Lamin B1
HIF-1α protein levels in RASMCs
I
RASMCs
DMSO
DHM
DMSO + TNF-α
DHM + TNF-α
HIF-1α
HO-1
DAPI
20 μm
Intensity (a.u.)
Distance (μm)
J
+TNF-α
DHM 0 0 1 5 20 μmol/L
HIF-1α
HO-1
Tubulin
Relative protein expression (fold of control)
0 μmol/L DHM
0 μmol/L DHM
1 μmol/L DHM
5 μmol/L DHM
20 μmol/L DHM
TNF-α
K
Hif1α mRNA levels in RASMCs
Vehicle
DHM
L
Hmox1 mRNA levels in RASMCs (fold of control)
M
ML385
LW6
DHM
HIF-1α
NRF2
HO-1
Tubulin
Control
DHM
ML385 + DHM
LW6 + DHM
Relative protein expression (fold of control)
N
Mouse Hmox1 promoter
Signal relative to Input (%)
IP: IgG HIF-1α
O
DMSO
DHM
Input
IgG
HIF-1α
bp

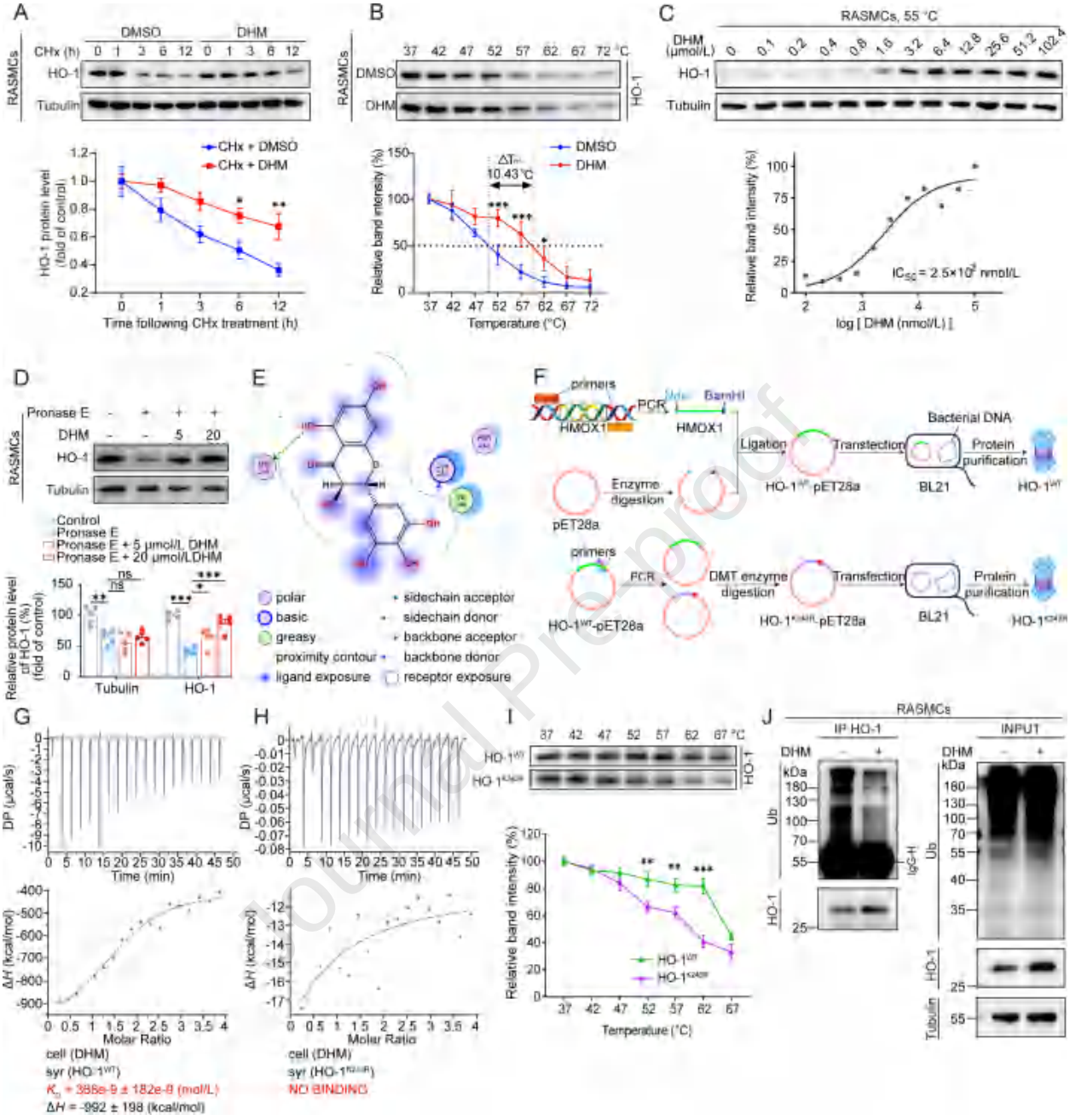

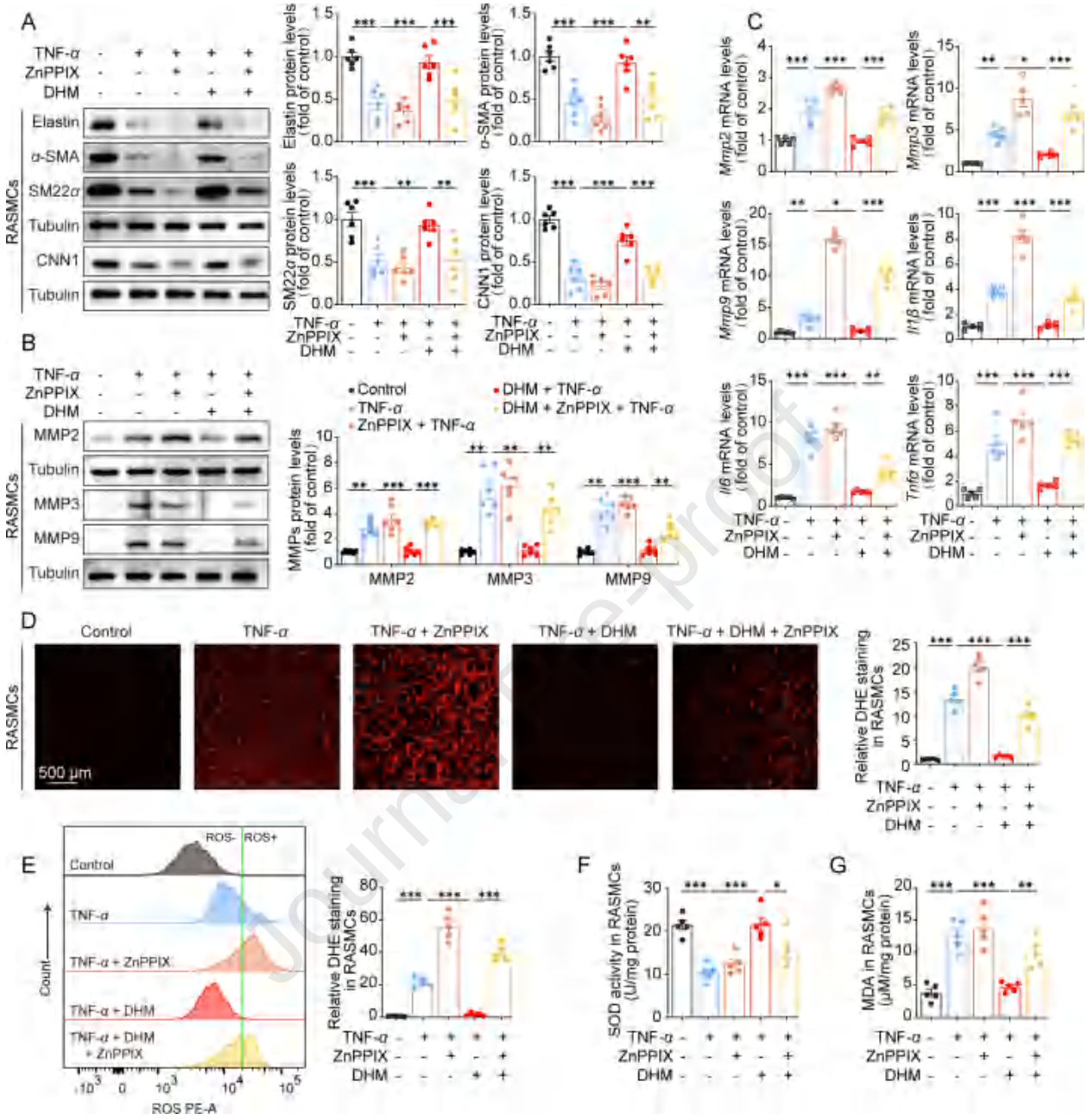
A
TNF-α
ZnPPIX
DHM
Elastin
α-SMA
SM22α
Tubulin
CNN1
Tubulin
RASMCs
Elastin protein levels (fold of control)
α-SMA protein levels (fold of control)
SM22α protein levels (fold of control)
CNN1 protein levels (fold of control)
B
MMP2
Tubulin
MMP3
MMP9
Tubulin
Control
TNF-α
ZnPPIX + TNF-α
DHM + TNF-α
DHM + ZnPPIX + TNF-α
MMPs protein levels (fold of control)
MMP2
MMP3
MMP9
C
Mmp2 mRNA levels (fold of control)
Mmp3 mRNA levels (fold of control)
Mmp9 mRNA levels (fold of control)
Il1β mRNA levels (fold of control)
Il6 mRNA levels (fold of control)
Tnfα mRNA levels (fold of control)
D
Control
TNF-α
TNF-α + ZnPPIX
TNF-α + DHM
TNF-α + DHM + ZnPPIX
RASMCs
500 μm
Relative DHE staining in RASMCs
E
ROS-
ROS+
Control
TNF-α
TNF-α + ZnPPIX
TNF-α + DHM
TNF-α + DHM + ZnPPIX
Count
ROS PE-A
Relative DHE staining in RASMCs
F
SOD activity in RASMCs (U/mg protein)
G
MDA in RASMCs (μM/mg protein)

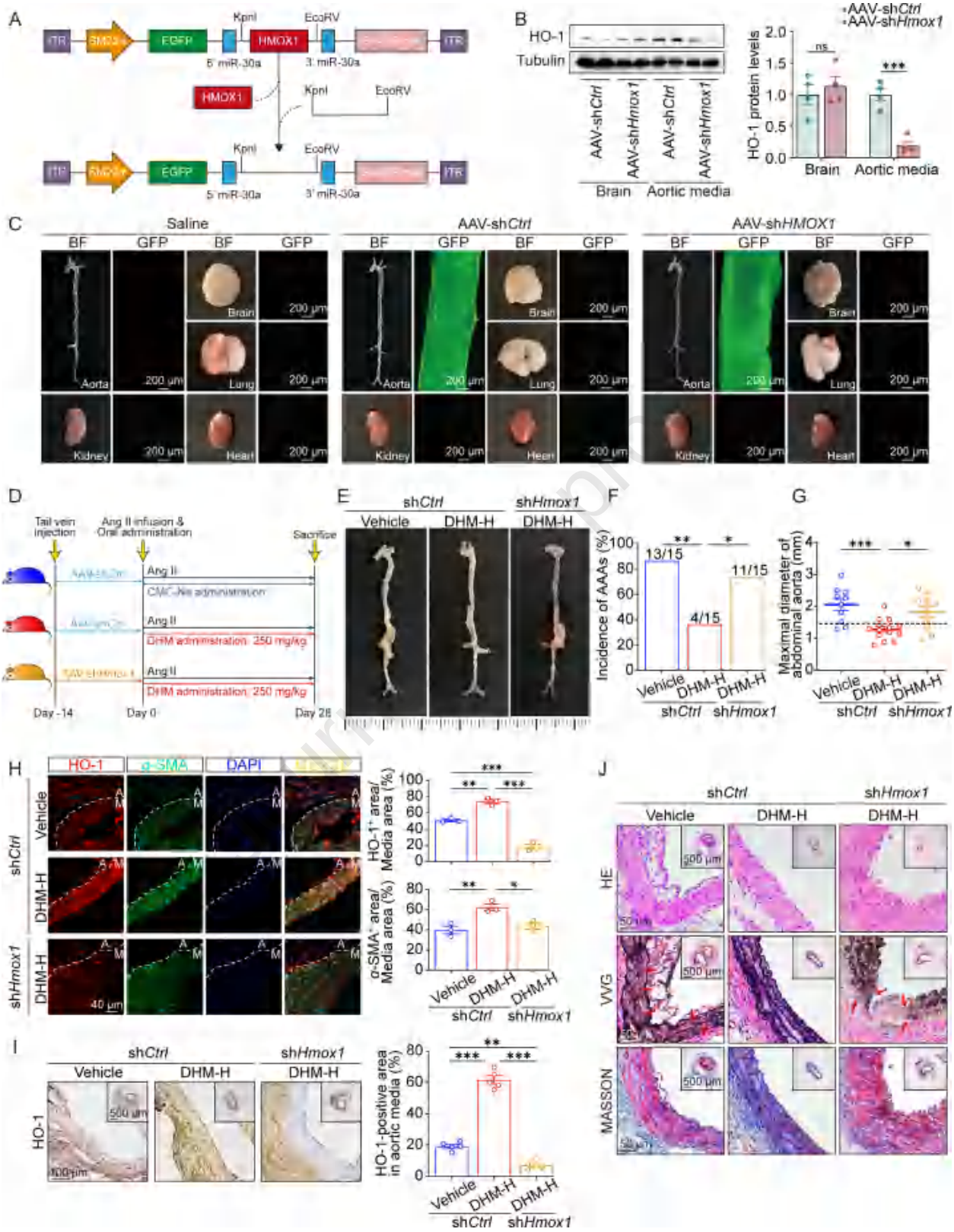
A
ITR
SM22α
EGFP
KpnI
HMOX1
EcoRV
5' miR-30a
3' miR-30a
B
HO-1
Tubulin
AAV-shCtrl
AAV-shHmox1
Brain
Aortic media
HO-1 protein levels
ns
***
C
Saline
AAV-shCtrl
AAV-shHMOX1
BF
GFP
Aorta
Brain
Lung
Kidney
Heart
200 μm
D
Tail vein injection
Ang II infusion & Oral administration
Sacrifice
Ang II
CMC-Na administration
DHM administration: 250 mg/kg
Day -14
Day 0
Day 28
E
shCtrl
shHmox1
Vehicle
DHM-H
F
Incidence of AAAs (%)
13/15
4/15
11/15
G
Maximal diameter of abdominal aorta (mm)
H
HO-1
α-SMA
DAPI
shCtrl
shHmox1
40 μm
HO-1+ area/ Media area (%)
α-SMA+ area/ Media area (%)
I
HO-1
500 μm
HO-1-positive area in aortic media (%)
J
HE
VVG
MASSON